Single-deletion-mutant, third-generation rabies viral vectors allow nontoxic retrograde targeting of projection neurons with greatly increased efficiency

Lei Jin[1], Heather A. Sullivan[1], Mulangma Zhu[1], Nicholas E. Lea[1], Thomas K. Lavin[1], Makoto Matsuyama[1], YuanYuan Hou[1], and Ian R. Wickersham[1]*

1. McGovern Institute for Brain Research, Massachusetts Institute of Technology, Cambridge, MA, USA
*Correspondence.

SUMMARY

Rabies viral vectors have become important components of the systems neuroscience toolkit, allowing both direct retrograde targeting of projection neurons and monosynaptic tracing of inputs to defined postsynaptic populations, but the rapid cytotoxicity of first-generation (ΔG) vectors limits their use to short-term experiments. We recently introduced second-generation, double-deletion-mutant (ΔGL) rabies viral vectors, showing that they efficiently retrogradely infect projection neurons and express recombinases effectively but with little to no detectable toxicity; more recently, we have shown that ΔGL viruses can be used for monosynaptic tracing with far lower cytotoxicity than the first-generation system. Here we introduce third-generation (ΔL) rabies viral vectors, which, like first-generation vectors, have only a single gene deleted from their genomes (in this case the viral polymerase gene L) but which appear to be as nontoxic as second-generation ones: using longitudinal structural and functional two-photon imaging in mouse visual cortex *in vivo*, we found that they did not kill labeled neurons or noticeably perturb their response properties over the entire months-long courses of imaging. Although third-generation vectors are therefore phenotypically very similar to second-generation ones, we show that they have the major advantage of growing to much higher titers, and this key difference results in 25% - 525% increased numbers of retrogradely labeled neurons *in vivo*. These ΔL rabies viral vectors therefore constitute a new state of the art for minimally perturbative, pathway-specific expression of recombinases and transactivators in mammalian neurons selected on the basis of their axonal projections. Because replication of deletion-mutant rabies viruses within complementing cells is precisely the process that underlies monosynaptic tracing, the higher replication efficiency of this new class of rabies viral vectors furthermore suggests the potential to provide the foundation of an improved nontoxic monosynaptic tracing system.

INTRODUCTION

Since their introduction to neuroscience in 2007 (Wickersham et al., 2007a; Wickersham et al., 2007b), recombinant rabies viral vectors have become widely-adopted tools in neuroscience, allowing "monosynaptic tracing" of direct inputs to genetically-targeted starting postsynaptic neuronal populations (Jin et al., 2021b; Wall et al., 2010; Wickersham et al., 2007b) as well as simple retrograde targeting of projection neurons when injected at the sites of these projection neurons' axonal arborizations (Chatterjee et al., 2018; Wickersham et al., 2007a). These vectors are now used in a large number of laboratories worldwide and have contributed to many high-impact studies of a wide variety of neural systems (Foster et al., 2021; Miyamichi et al., 2011; Reardon et al., 2016; Schwarz et al., 2015; Siu et al., 2021; Smith et al., 2021; Stephenson-Jones et al., 2016; Wu et al., 2021; Yao et al., 2021).

Because first generation ("ΔG") rabies viral vectors (which have only the glycoprotein gene G deleted from their genomes) are cytotoxic (Chatterjee et al., 2018; Jin et al., 2021a; Jin et al., 2021b; Wickersham et al., 2007a), we recently introduced second-generation, "ΔGL" rabies viral vectors, which have both the glycoprotein gene G and the viral polymerase gene L (for "large" protein) deleted from their genomes (Chatterjee et al., 2018). Because the viral polymerase is absolutely required for transcription of all genes

from the rabies viral genome as well as for replication of the viral genome itself (Albertini et al., 2011; Finke and Conzelmann, 2005; Horwitz et al., 2020; Morin et al., 2013; Ogino and Green, 2019; Te Velthuis et al., 2021), this additional deletion, by design, reduces gene expression to a minimal level (provided by the few starting copies of the polymerase protein that are copackaged in each viral particle) that appears to be completely harmless to the "infected" cells. Because transgene expression is reduced by the same degree, we inserted the genes for Cre and Flpo recombinase, of which even low levels of expression are sufficient to cause neuroscientifically-useful downstream effects such as expression of fluorophores or calcium indicators in labeled cells (Chatterjee et al., 2018). We originally showed that these ΔGL vectors are useful tools for retrograde targeting of projection neurons (Chatterjee et al., 2018), and they have since been used as such for applications including optogenetics and transcriptomic profiling (Ren et al., 2021; Roy et al., 2021; Tasic et al., 2018). More recently, we have also shown that ΔGL vectors can be complemented *in vivo* by expression of both G and L *in trans*, yielding a second-generation monosynaptic tracing system with far lower cytotoxicity than the first-generation version (Jin et al., 2021a).

Here we show that deletion of L alone appears to make rabies viral vectors as nontoxic as ΔGL ones, with labeled neurons surviving for at least months with apparently unperturbed visual response properties. We find that these ΔL vectors have a major growth advantage over ΔGL ones in cell culture, attaining much higher titers in complementing cells in culture. This higher replication efficiency translates into the practical advantage of retrogradely labeling many more projection neurons when injected into these neurons' target sites *in vivo*.

RESULTS

Construction and characterization of ΔL rabies virus

We began by constructing rabies viral vectors with only the polymerase gene deleted and characterized their gene expression levels and growth dynamics in cell culture (Figure 1). Beginning with the genome plasmid of a ΔGL virus (Chatterjee et al., 2018), we reinserted the native glycoprotein gene in its original location, followed by the gene for Cre recombinase (codon-optimized for mouse (Koresawa et al., 2000)) in an additional transcriptional unit, then produced infectious virus by standard techniques (see Methods). We then compared the gene expression levels of the resulting virus, RVΔL-Cre, to those of first- and second-generation versions (RVΔG-Cre and RVΔGL-Cre, respectively) in cell culture (HEK 293T/17 cells) using immunostaining for Cre as well as for the viral nucleoprotein, the highest-expressed rabies viral protein.

As shown in Figure 1A-D, whereas the first-generation (ΔG) virus expressed high levels of nucleoprotein (which accumulated in cytoplasmic inclusions) and Cre (which localized to the nuclei), the ΔGL and ΔL viruses had very low expression levels of both Cre and nucleoprotein, with the amount of label for these proteins appearing much more similar to that seen in uninfected control cells than in cells infected with the ΔG virus. We also found similarly low transgene expression levels for ΔL and ΔGL viruses expressing EGFP (Figure S1). However, just as we found previously for ΔGL viruses (Chatterjee et al., 2018), the Cre expressed by RVΔL-Cre was sufficient to result in bright labeling of Cre reporter cells (bottom row in panels A-D).

These results led us to predict that ΔL viruses would be as nontoxic as ΔGL ones, because of their similarly low expression levels, and also that they would be similarly able to recombine reporter alleles *in vivo* in order to allow downstream expression of useful transgene products such as fluorophores, activity indicators, or opsins.

It remained to be seen, however, whether ΔL viruses would have any particular advantage over ΔGL ones for purposes of retrogradely targeting neurons. Specifically, if they could not be produced at significantly higher titers, they could be expected to label similar numbers of projection neurons, making ΔL vectors a mere curiosity of purely academic interest and with no relevance to neuroscientists. However, if they could be grown to much higher titers than ΔGL vectors, that could be expected to translate to the ability to retrogradely label many more projection neurons, a desirable characteristic indeed for a tool for retrograde targeting.

To examine this, we directly compared the ability of ΔL virus to replicate in complementing cells with that of ΔGL and ΔG viruses (Figure 1E-F). We infected cell lines expressing L, G, or both with the three different generations of virus, at two different multiplicities of infection (MOI, measured in infectious units per cell): either very low (MOI = 0.01, "multi-step growth curves" (Gomme et al., 2010; Wang and Bushman, 2006)) or high (MOI = 1, "single-step growth curves". Following a one-hour incubation in the presence of the

viruses, we washed the cells twice with DPBS and applied fresh medium, then collected supernatant samples every 24 hours for five days after infection, then titered the samples on reporter cells.

As seen in Figure 1E-F, the results were clear: whereas the ΔGL virus (on cells expressing both G and L) never accumulated to titers higher than 2.37e6 iu/mL in either experiment, the ΔL virus grew to maximal titers of 6.51e6 iu/mL (at MOI of 0.01) and 1.96e7 iu/mL (at MOI of 1) on the same cell line (expressing both G and L) and considerably higher (maximal titers of 1.31e7 iu/mL at MOI=0.01 and 2.60e7 iu/mL at MOI=1) on cells expressing L alone. The ΔG virus grew to similarly high (or slightly higher, in the MOI=1 case) titers to the ΔL one: 6.83e6 iu/mL at MOI=0.01 and 3.03e7 iu/mL at MOI=1, suggesting that single-deletion-mutant rabies viruses may in general be easier to make at high titers than viruses with multiple deleted genes. In non-complementing cells, by contrast, no such replication of any of these viruses (ΔL, ΔGL, or ΔG) occurred (Figure S2).

These findings that a ΔL rabies virus could be grown to 11-fold higher titer than a matched ΔGL one led us to predict that ΔL viruses would be superior tools for retrograde targeting *in vivo*, because their much higher titers would result in retrograde infection of many more projection neurons.

Retrograde targeting *in vivo*

To test this prediction, we made matched preparations of ΔGL and ΔL viruses expressing either Cre or Flpo (mouse-codon-optimized Flp recombinase (Raymond and Soriano, 2007)), then injected each of the four viruses in the somatosensory thalami of reporter mice (Ai14 (Madisen et al., 2010) for the Cre viruses, Ai65F (Daigle et al., 2018) for the Flpo ones; both lines express tdTomato following recombination by the respective recombinase). We sacrificed the mice at either 7 days or 4 weeks after injection, sectioned and imaged the brains by confocal microscopy, and counted the numbers of retrogradely labeled cells in cortex. Figure 2 shows the results.

As seen in panels 2B-E, for both recombinases, and at both timepoints, the ΔL viruses significantly outperformed the ΔGL ones. For the Flpo viruses, the difference was dramatic: at the 1-week timepoint, the ΔL virus labeled 24 times as many cells as the ΔGL one (although this difference was not statistically significant due to high variance in the ΔL cohort: single factor ANOVA, p=0.275, n = 8 mice each group); by the 4-week timepoint, the ΔL-Flpo virus had labeled 6.25 times as many cells as the ΔGL counterpart, a difference that was extremely significant (single factor ANOVA, p=3.21E-04, n = 8 mice each group). For the Cre viruses, the difference was smaller, presumably due a ceiling effect (see Discussion), but still highly significant: at 1 week, the ΔL-Cre virus had labeled 1.40 times as many cells as ΔGL-Cre (single factor ANOVA, p=4.20E-03; n = 4 mice each group); at the 4-week timepoint, the ΔL-Cre virus had labeled 1.25 times as many cells as ΔGL-Cre (single factor ANOVA, p=7.38E-04, n = 4 mice per group).

We also made some injections of RVΔL-Cre, in thalami of Ai14 mice, with the much longer survival times of 4 or 6 months (Fig 2F-G). The results at both of these longer survival times appeared very similar to those at the shorter ones. Consistent with extensive prior literature on corticothalamic neurons (Alitto and Usrey, 2003; Rockland, 2021; Rouiller and Welker, 2000) and with our previous results with corticothalamic injections of ΔG and ΔGL viruses (Chatterjee et al., 2018; Wickersham et al., 2007a), the cells labeled in cortex by both viruses at all timepoints were pyramidal neurons in layer 6, with a few in layer 5. Furthermore, labeled neurons all appeared morphologically normal even months after injection, with the fine processes of axons and dendrites, including individual spines (rightmost images in 2F-G) clearly visible and without blebbing or other obvious abnormalities.

As a further test of the flexibility of ΔL vectors, we made a version expression the tetracycline transactivator (tTA) and injected it in the thalamus of Ai63 reporter mice (in which TRE-tight drives tdTomato expression) (Daigle et al., 2018). As seen in Figure S3, thousands of cortical thalamic cells were found retrogradely labeled at both 1-week and 4-week survival times, with no significant difference between the numbers at the two timepoints (single factor ANOVA, p = 0.772, n = 4 mice per group).

Longitudinal structural two-photon imaging *in vivo*

Because examining only postmortem tissue can be very misleading when attempting to determine whether a virus is nontoxic (see Jin et al. '21 (Jin et al., 2021a) for a detailed case study), we conducted longitudinal two-photon imaging of RVΔL-labeled neurons *in vivo* (Figure 3). We injected either RVΔGL-Cre (Chatterjee et al., 2018) or RVΔL-Cre in primary visual cortex (V1) of Ai14 reporter mice, then imaged the resulting tdTomato-expressing neurons at or near the injection site beginning 7 days after injection and continuing every 7 or 14 days until 16 weeks postinjection. As seen in Figure 3, the results using the two viruses were very similar. For both ΔGL and ΔL viruses, the numbers of visibly labeled neurons increased significantly

between 1 week and 4 weeks postinjection (Figure 3D, G), by 56.27% for ΔGL and by 67.77% for ΔL (paired t-tests, p = 1.319E-04 for ΔGL, p = 1.003E-05 for ΔL, n = 8 FOVs for each virus). Also for both viruses, the numbers of visibly labeled neurons remained nearly completely constant from the 4-week timepoint onward through all remaining imaging sessions (Figure 3E, H) (with the number of labeled cells at the 4-week timepoint being not significantly different than that at the 12-week timepoint for the ΔL virus (paired t-test, p = 0.1327, n = 8 FOVs) and slightly (0.5%) lower for the ΔGL virus (paired t-test, p = 0.0056, n = 8 FOVs). See File S3 for all counts and statistical comparisons; see also Video S1 for a rendering of a group of ΔL-labeled neurons at 2 weeks and again at 10 weeks.

Longitudinal functional two-photon imaging *in vivo*

We went on to examine the functional properties of RVΔL-labeled neurons *in vivo*. As for the structural imaging (see above), we injected RVΔL-Cre in the primary visual cortices of reporter mice, in this case mice that express the calcium indicator GCaMP6s (Chen et al., 2013) after Cre recombination (Figure 4). Beginning one week later, we began imaged the calcium signals in the labeled neurons in a series of imaging sessions that continued until 16 weeks postinjection, in the awake mice viewed visual stimuli consisting of drifting gratings of different orientations and frequencies. Just as we found previously for ΔGL viruses (Chatterjee et al., 2018; Jin et al., 2021b), we found no signs of dysfunction in cells labeled by the third-generation vector for as long as we followed them (Figure 4; see also Figures S4 and S5. See File S4 for all counts and statistical comparisons and Video S2 for an example of calcium responses in a group of cortical neurons 16 weeks after injection of RVΔL-Cre).

DISCUSSION

Here we have shown that deletion of just the polymerase gene renders rabies viral vectors nontoxic, like second-generation (ΔGL) vectors, but makes them much more efficient at replicating within complementing cells in culture. This ability to be grown to much higher titers results in significantly increased transduction of projection neurons within a given pathway. This more comprehensive access to projection neurons will increase the yield and efficacy of systems neuroscience experiments that depend on the retrograde targeting approach.

In the corticothalamic pathway that we have examined here, the advantage of a ΔL vector over the ΔGL equivalent was clearest in the case of the Flpo-expressing versions, with the ΔL vector labeling 6.25 times as many neurons as the ΔGL one did at four weeks postinjection. This ratio is of the same order of magnitude as the ratio of the titers of the injected Flpo viruses (14.4: see Methods). By contrast, for the Cre-expressing versions, the advantage of the ΔL vector over the ΔGL one was more modest, labeling 1.25 times as many cells, even though the ratio of the titers of these Cre vectors was even higher (20.5). Because the absolute numbers of retrogradely labeled neurons, as well as the titers, were much higher for the Cre viruses than for the corresponding Flpo ones, we presume that the smaller advantage of the ΔL version seen in this case was because of a ceiling effect, with the ΔGL-Cre virus already labeling most of the available neurons in this pathway.

One could certainly argue that the much higher titers that we are easily able to obtain with ΔL vectors could also, in theory, potentially be achieved with ΔGL vectors, if enough effort were put into generating and testing producer cell lines expressing both G and L in order to find one that expressed the two genes at just the right ratio and levels. In practice, however, this hypothetical future research effort does not detract from the fact that the best currently-existing preparations of ΔL rabies viral vectors label many more cells than do ΔGL ones, making them the better choice for retrograde targeting applications.

We note that, although here we have only demonstrated the use of ΔL rabies viral vectors in mice, they are also highly likely to work in a wide variety of mammalian species, because, apart from their shorter RNA genomes, the structural properties of second- and third-generation rabies viral particles are identical to those of first-generation ones, which have been successfully used in diverse mammalian species including rats (Cruz et al., 2021), cats (Connolly et al., 2012; Liu et al., 2013), ferrets (Hasse et al., 2019), and macaques (Bragg et al., 2017; Briggs et al., 2016; Lyon et al., 2010; Nassi and Callaway, 2006, 2007; Nassi et al., 2006; Siu et al., 2021; Yarch et al., 2017) (and even in fish (Dohaku et al., 2019; Satou et al., 2021; Zhu et al., 2009) and frogs (Faulkner et al., 2021)).

Our findings here that ΔL rabies viruses have extremely low expression levels and do not replicate within (or spread beyond, *in vivo*) non-complementing cells are entirely consistent with similar findings in cell culture in a recent report on an L-deficient rabies virus encoding firefly luciferase (Nakagawa et al., 2017).

A note about safety: our results strongly suggest that ΔL rabies viruses are unable to replicate in the absence of complementation and moreover are harmless to any cells that they transduce. However, a mixture of ΔL and ΔG viruses could pose a safety risk, because such viruses will be mutually complementary. Care must therefore be taken to avoid contamination between ΔL and ΔG constructs – either packaged viruses or the genome plasmids used to make them – which would have the potential to create a self-complementing replication-competent mixture (see Hidaka et al. (Hidaka et al., 2018) for an example of such a self-complementing mixture).

Finally, we have recently shown (Jin et al., 2021b) that second-generation (ΔGL) rabies viral vectors can spread transsynaptically when complemented by provision of both G and L *in trans*. That is, complementation of an L-deficient rabies virus (in that case, a G- and L-deficient virus that is also complemented by G) allows it to spread beyond initially infected cells *in vivo*. It is therefore reasonable to infer that provision of L *in trans* should allow third-generation, ΔL rabies viral vectors to spread beyond initially infected cells, given that we have shown here that such complementation in cell culture allows ΔL viruses to replicate very efficiently. We have also shown here, with the longitudinal two-photon imaging of labeled neurons, that ΔL viruses do not spread beyond initially infected cells *in vivo* in the absence of complementation. Collectively, our results therefore suggest the outlines of a third-generation monosynaptic tracing system based on ΔL vectors complemented with L expression *in trans*. However, genetic targeting of a ΔL vector to specific starting cell types might appear elusive: in the first- and second-generation systems (Jin et al., 2021b; Wickersham et al., 2007b), this targeting is achieved by packaging the rabies viral particles with an avian retroviral envelope protein (EnvA) instead of its own envelope glycoprotein, so that they can only infect cells that have been engineered to express EnvA's cognate receptor. On the face of it, this pseudotyping strategy requires that G be deleted from the rabies viral genome, because expression of G by the virus within the EnvA-expressing producer cells would result in the production of virions with membranes populated by a mixture of EnvA and the rabies viral glycoprotein. If this challenge could be overcome, our present findings that ΔL viruses replicate more readily in complementing cells, which is the fundamental process central to monosynaptic tracing (Wickersham et al., 2007b), suggest that a third-generation monosynaptic tracing system could be more efficient than the second-generation one.

METHODS

All experiments involving animals were conducted according to NIH guidelines and approved by the MIT Committee for Animal Care. Mice were housed 1-5 per cage under a normal light/dark cycle for all experiments.

Cloning

The third-generation rabies viral vector genome plasmids pRVΔL-5Cre, pRVΔL-5Flpo, and pRVΔL-5tTA (Addgene 182964, 182965, and 182966) (the "5" denoting the position of the transgene relative to the other genes in the viral genome) was made by replacing the mCre gene in pRVΔGL-4Cre (Chatterjee et al., 2018) (Addgene 98039) with the SAD B19 glycoprotein gene from pCAG-B19G (Chatterjee et al., 2018) (Addgene 59921) and either the mCre, Flpo (from pRVΔG-4Flpo (Addgene 98040)), or tTA (from pAAV-syn-FLEX-splitTVA-EGFP-tTA (Liu et al., 2017) (Addgene 100798)) gene, separated by endogenous rabies viral transcriptional stop and start signals, using seamless cloning (InFusion (Takara) or HiFi (NEB)).

The piggyBac vector pB-TREtight-EGFP (Addgene 182967) was made by cloning the TRE-tight element from pAAV-TREtight-mTagBFP2-B19G (Liu et al., 2017) and the EGFP gene into pB-CAG-TEVp-IRES-mCherry (Addgene 174377) in place of the CAG-TEVp-IRES-mCherry sequences using HiFi seamless cloning (NEB).

The piggyBac plasmid pB-CAG-B19G-IRES-EGFP-WPRE-BGHpA (Addgene 178517) was made by cloning the CAG promoter from pCAG-B19G (Addgene 59921), the SAD B19 L gene, the EMCV IRES (Gallardo et al., 1997), the mCherry (Shaner et al., 2004) gene, and the woodchuck post-transcriptional regulatory element and bovine growth hormone polyadenylation signal from pCSC-SP-PW-GFP (Addgene 12337), into PB-CMV-MCS-EF1-Puro (System Biosciences #PB510B-1).

Cell lines

The BHK-B19G3 cell line, expressing the SAD B19 strain rabies virus glycoprotein gene, was made by resorting BHK-B19G2 cells (Wickersham et al., 2010) on a BD Facs Aria cell sorter and retaining the

brightest 2% of EGFP-positive cells as well as the next-brightest 18%. Following the sort, both populations were expanded and refrozen, then thawed and tested for their efficacy at supporting replication of ΔG virus; the second-brightest population ("BHK-B19G3_2") was found to result in higher titers and is referred to here as BHK-B19G3.

The BHK-B19L cell line, expressing the SAD B19 strain rabies virus polymerase gene, was made by transfecting BHK-21 cells (ATCC CCL-10) with pCAG-hypBase (Jin et al., 2021a) and pB-CAG-B19L-IRES-mCherry-WPRE-BGHpA (Jin et al., 2021b) using Lipofectamine 2000 (Thermo Fisher 11668019), then expanding the cells and sorting on a FACS Aria sorter (BD) to collect the brightest 5%, as well as the next brightest 5%, of mCherry-expressing cells. The two collected populations were expanded and refrozen, then thawed and tested for their efficacy at supporting replication of ΔL virus; the second-brightest population ("BHK-B19L_2") was found to result in higher titers and is referred to here as BHK-B19L.

The BHK-B19L-G cell line, expressing the SAD B19 strain rabies virus polymerase and glycoprotein genes, was made by transfecting BHK-B19L cells (see above) with pCAG-hypBase and pB-CAG-B19G-IRES-EGFP-WPRE-BGHpA (see above), then expanding and sorting on a BD FACS Aria, keeping the brightest 5%, as well as the next brightest 5%, of EGFP-expressing cells which also expressed mCherry. The sorted cells were expanded and refrozen, then thawed and tested for their efficacy at supporting replication of ΔGL virus; the brightest population ("BHK-B19L-G_1") was found to result in higher titers and is referred to here as BHK-B19L-G.

The 293T-TREtight-EGFP cell line for titering tTA-expressing viruses was made by transfecting HEK 293T/17 cells with pCAG-hypBase and pB-TREtight-EGFP (described above), then expanded and sorted on a BD FACS Aria, excluding the brightest 2% of EGFP cells, and keeping four of the next brightest EGFP cell populations. The sorted cells were expanded, frozen, and then thawed for testing their efficacy at titering ΔL-tTA virus. The fourth-brightest tranche of cells was used for subsequent titering of ΔL-tTA virus.

Rabies virus production and titering

The first-generation vector RVΔG-4Cre, the second-generation vectors RVΔGL-4Cre and RVΔGL-4Flpo, and the third-generation vectors RVΔL-5Cre, RVΔL-5Flpo, and RVΔL-5tTA were rescued as described previously (Chatterjee et al., 2018) using genome plasmids pRVΔGL-4Cre, pRVΔGL-4Flpo, pRVΔL-5Cre, pRVΔL-5Flpo, and pRVΔL-5tTA, respectively. For simplicity, these viruses are referred to in this manuscript as RVΔG-Cre, RVΔGL-Cre, RVΔGL-Flpo, RVΔL-Cre, RVΔL-Flpo, and RVΔL-tTA, omitting the numbers denoting the positions of the transgenes within the viral genomes. Rescue supernatants were collected and filtered as described (Wickersham and Sullivan, 2015), titered on the reporter cell lines 293T-FLEX BC (for Cre viruses) or 293T-F14F15S-BC (for Flpo viruses) (Jin et al., 2021a) as described (Wickersham et al., 2010), then used to infect BHK-B19G3, BHK-B19L-G, or BHK-B19L cells (see above) at multiplicities of infection ranging from 0.1 to 1. Supernatants from these "P1" plates were collected and titered as described (Wickersham and Sullivan, 2015); in some cases, these were used for a similar second passage ("P2"). Purification and concentration of either P1 or P2 supernatants was as described (Wickersham et al., 2010), with supernatants treated with benzonase (Sigma 71206) (25 minute incubation at 37°C with 30 units/ml at) before ultracentrifugation. Concentrated viruses were aliquoted and frozen at -80°C. Rabies viruses were titered on reporter cells (293T-FLEX-BC for Cre viruses, 293T-F14F15S-BC for Flpo viruses, 293T-TREtight-EGFP (see above) for RVΔL-tTA) as described (Wickersham et al., 2010), using a LUNA-II cell counter (Logos Biosystems) instead of a hemocytometer for counting cells, and in some cases using two-fold (as opposed to ten-fold) dilution series for more precise comparisons of titers.

Immunostaining, imaging, and flow cytometry of cultured cells

For anti-nucleoprotein and anti-Cre staining (for Figure 1): HEK 293T/17 (ATCC 11268) cells were plated on poly-L-lysine-coated coverslips in 24-well plates, then infected the following day with serial dilutions of RVΔG-4Cre (Chatterjee et al., 2018), RVΔGL-4Cre (Chatterjee et al., 2018), or RVΔL-5Cre. Three days after infection, cells were fixed with 2% paraformaldehyde, washed repeatedly with blocking/permeabilization buffer (0.1% Triton-X (Sigma) and 1% bovine serum albumin (Sigma) in PBS), then labeled with a 1:100 dilution of anti-nucleoprotein monoclonal antibody blend (Light Diagnostics Rabies DFA Reagent, EMD Millipore 5100) as well as a 1:250 dilution of rabbit anti-Cre polyclonal antibody (Millipore Sigma 69050) followed by a 1:200 dilution of Alexa Fluor 594-conjugated donkey anti-rabbit secondary (Jackson Immuno 711-585-152).

For anti-EGFP staining (for Figure S1), HEK cells were plated as above, then infected the following day with serial dilutions of RVΔG-4EGFP (Wickersham et al., 2010), RVΔGL-4EGFP (Chatterjee et al., 2018), or RVΔL-5EGFP, with immunostaining three days postinfection, using a 1:1000 dilution of chicken anti-GFP polyclonal antibody (Aves Labs, GFP-1020) and a 1:500 dilution of Alexa Fluor 594-conjugated donkey anti-chicken secondary antibody (Jackson Immuno 703-585-155).

Immunostained cells on coverslips were mounted on slides using Prolong Diamond Antifade mounting medium (Thermo P36970) and imaged on a Zeiss LSM 900 confocal microscope using a 20x objective.

For matched flow cytometric analysis of immunostained cells, cells were plated in 24-well plates without poly-L-lysine-coated coverslips but otherwise immunostained as described above, then analyzed on an LSR II flow cytometer (BD) using FACS Diva software (BD). Histograms displayed in Figure 1 were smoothed using the FACS Diva "Smooth histogram" setting.

Viral growth analysis

For determining growth curves, BHK-B19G3, BHK-B19L-G, and BHK-B19L cells (see above) were plated in 10 cm plates coated in poly-L-lysine in normal medium (10% fetal bovine serum (VWR 16777-014) and antibiotic-antimycotic (Thermo 15240096) in DMEM (Thermo 11995073)) (Wickersham et al., 2010). The following day, cells were infected with RVΔG-4Cre(B19G), RVΔGL-4Cre(B19G), or RVΔL-5Cre(B19G) at an MOI of either 1 (for single-step growth curves) or 0.01 (for multi-step growth curves), with viruses diluted in normal medium at a total volume of 2 ml per plate, with each condition in triplicate. Following a one-hour incubation, the virus-containing medium was aspirated, plates were washed twice in DPBS (Thermo 14190144), and 12 ml fresh medium was added to each plate before they were returned to the incubator. Every 24 hours for the following five days, 200 µl of supernatant was collected from each plate; these supernatant samples were filter-sterilized using a 96-well 0.45um PVDF filter plate (Millipore MSHVN4510), then frozen at -80°C before all samples were thawed and titered on HEK 293T-FLEX-BC cells as described above.

Mouse strains

The Cre-dependent tdTomato reporter line Ai14 (Madisen et al., 2010) was purchased from Jackson Laboratory (catalog # 007914). The Flp-dependent tdTomato reporter line Ai65F was obtained by crossing the Cre- and Flp-dependent tdTomato double-reporter line Ai65D (Madisen et al., 2015) (Jackson Laboratory 021875) to the Cre deleter line Meox2-Cre (Tallquist and Soriano, 2000) (Jackson Laboratory 003755), then breeding out the Meox2-Cre allele. An equivalent Ai65F line, made using a different Cre deleter line, was described in Daigle et al. '18 (Daigle et al., 2018) and is now available from Jackson Laboratory (catalog # 032864). The tTA-dependent tdTomato reporter line Ai63 (Daigle et al., 2018) was a generous gift from Hongkui Zeng and Tanya Daigle. Mice used for the functional two-photon imaging experiments were crosses of the Cre- and tTA-dependent GCaMP6s line Ai94D (Jackson Laboratory 024104) with the Cre-dependent tTA line ROSA:LNL:tTA (Wang et al., 2008) (Jackson Laboratory 011008). All mice were maintained in a C57BL/6J (Jackson Laboratory 000664) background.

For experiments, adult mice of both sexes were used, of the following mouse strains. For retrograde targeting using Cre-expressing viruses (Figure 2) and structural two-photon imaging (Figure 3): Ai14 heterozygotes. For retrograde targeting using Flpo-expressing viruses (Figure 2): Ai65F heterozygotes. For retrograde targeting using RVΔL-tTA (Figure S3): Ai63 heterozygotes. For functional two-photon imaging (Figures 4, S4, and S5): Ai94D x ROSA:LNL:tTA double homozygotes.

Stereotaxic injections

200 nl of rabies virus was injected into either somatosensory thalamus (VPM/Po, for figure 2) or primary visual cortex (for two-photon experiments) of anesthetized adult mice using a stereotaxic instrument (Stoelting Co., 51925) and a custom injection apparatus consisting of a hydraulic manipulator (Narishige, MO-10) with headstage coupled via custom adaptors to a wire plunger advanced through pulled glass capillaries (Drummond, Wiretrol II) back-filled with mineral oil and front-filled with viral vector solution (Lavin et al., 2019). We have described this injection system in detail previously. Injection coordinates for VPM/Po were: anteroposterior (AP) = -1.82 mm with respect to (w.r.t.) bregma, lateromedial (LM) = +1.54 mm w.r.t bregma, dorsoventral (DV) = -3.15 mm w.r.t the brain surface; injection coordinates for V1 cortex were: AP = -2.70 mm w.r.t. bregma, LM = 2.50 mm w.r.t. bregma, DV = -0.26 mm w.r.t the brain surface.

For mice to be used for two-photon imaging, a 3 mm craniotomy was opened over primary visual cortex (V1). Glass windows composed of a 3mm-diameter glass coverslip (Warner Instruments CS-3R) glued (Optical Adhesive 61, Norland Products) to a 5mm-diameter glass coverslip (Warner Instruments CS-5R) were affixed over the craniotomy with Metabond (Parkell) after virus injection.

For the ΔGL vs. ΔL experiments (Figure 2), the four viruses were produced in parallel for direct comparison, and RVΔL-Cre (6.16E+10 i.u./ml) or RVΔGL-Cre (3.01E+09 i.u./ml) was injected into Ai14 (het) mice, and RVΔL-Flpo (1.61E+09 i.u./ml) or RVΔGL-4Flpo (1.12E+08 i.u./ml) was injected into Ai65F (het) mice. For the 4-month and 6-month experiments for Figure 2, RVΔL-Cre (1.66E+10 i.u./ml) was injected into Ai14 (het) mice. For Figure S3, RVΔL-tTA (3.63E+10 iu/ml) was injected into Ai63 (het) mice.

For two-photon structural experiments (Figure 3), RVΔGL-Cre (1.19E+10 iu/ml) or RVΔL-Cre (1.66E+10 iu/ml diluted to 1.19E+10 iu/ml for matching to RVΔGL-Cre) was injected into Ai14 (het) mice. For two-photon functional experiments in Figure 4, RVΔL-Cre (2.61E+10 iu/ml) was injected into homo/homo Ai94D x ROSA:LNL:tTA mice.

Perfusions, histology, and confocal imaging

1 week to 6 months (see main text) after injection of rabies virus, anesthetized mice were transcardially perfused with 4% paraformaldehyde. Brains were postfixed overnight in 4% paraformaldehyde in PBS on a shaker at 4°C and cut into 50 µm coronal sections on a vibrating microtome (Leica, VT-1000S). Sections were collected sequentially into 6 tubes containing cryoprotectant, so that each tube contained every sixth section, then frozen at -20°C. Sections to be imaged were washed to remove cryoprotectant, then mounted with Prolong Diamond Antifade mounting medium (Thermo Fisher P36970) and imaged on a confocal microscope (Zeiss, LSM 900). To ensure that the confocal images included in the figures are representative of each group, the images were taken after the counts were conducted, and the mouse with the next higher number of labeled neurons than the average number for its group was selected for confocal imaging.

Quantification of retrograde targeting

Coronal sections between 0.43mm anterior and 4.07mm posterior to bregma were imaged with an epifluorescence microscope for cell counting (Zeiss, Imager.Z2). Due to the high density of retrogradely labeled tdTomato neurons in the cortex at the injection site (VPM/Po), cells were counted using the Analyze Particle function in ImageJ (size in micron^2: 20-400; circularity: 0.20-1.00). Only one of the six series of sections (i.e., every sixth section: see above) was counted for each mouse. P-values for all comparisons were obtained using single-factor ANOVAs.

Structural two-photon imaging and image analysis

Beginning seven days after injection of each rabies virus and recurring at the subsequent indicated timepoints (see main text) up to a maximum of 16 weeks following rabies virus injection, fields of view (FOVs) were imaged on a Prairie/Bruker Ultima IV In Vivo two-photon microscope driven by a Spectra Physics Mai-Tai Deep See laser with a mode locked Ti:sapphire laser emitting at a wavelength of 1020 nm for excitation of tdTomato. In order to distinguish individual labeled neurons, FOVs were chosen some distance away from the area of brightest tdTomato labeling. Two well-separated areas were chosen in each mouse. For each imaging session, mice were reanesthetized and mounted via their headplates to a custom frame, with ointment applied to protect their eyes and with a handwarmer maintaining body temperature. Imaging parameters were as follows: image size 512 X 512 pixels (282.6 µm x 282.6 µm), 0.782 Hz frame rate, dwell time 4.0 µs, 2x optical zoom, Z-stack step size 1 µm. Image acquisition was controlled with Prairie View 5.4 software. Laser power exiting the 20x water-immersion objective (Zeiss, W plan-apochromat, NA 1.0) varied between 20 and 65 mW depending on focal plane depth (Pockels cell value was automatically increased from 450 at the top section of each stack to 750 at the bottom section). For the example images of labeled cells, maximum intensity projections (stacks of 100-200 µm) were made with ImageJ software. Cell counting was automated using the "Analyze Particles" function in ImageJ. Plots of cell counts were made with Prism 9 (GraphPad Software, San Diego, California).

Functional two-photon imaging and image analysis

For functional two-photon imaging of RVΔL-Cre-labeled cells, FOVs were slightly offset from the regions of brightest GCaMP6s label in left-hemisphere V1 in order to allow separate identification of individual cells. This imaging was performed using the same microscope (5.356-Hz frame rate, 1024X 128 pixels, 565.1

μm x 565.1 μm, dwell time 0.8 μs, 1x optical zoom, scan angle 45 degree) with the same objective and laser (at 920 nm) as for the structural imaging experiments. Laser power at the objective ranged from 10 to 65 mW. Calcium imaging data were acquired in supragranular layers (100 to 200 μm deep). Surface vasculature provided coarse fiducial markers for finding the same FOVs in different imaging sessions. For these experiments, mice were awake and head-fixed. No behavioral training or reward was given. Visual stimuli were generated in Matlab (R2015R version) with custom software based on Psychtoolbox (http://psychtoolbox.org) and shown on the same LCD screen as in the widefield mapping experiments. Each condition consisted of 2 s of a full-field sine wave grating drifting in one direction, presented at 80% contrast with spatial frequency of 0.04 cycles/ degree, followed by 2 s of uniform mean luminance (gray). All permutations of 12 directions (30° steps) and 5 temporal frequencies (1, 2, 4, 8 and 15 Hz) were shown, in randomized order. The complete set was repeated 10 times, for a total stimulation period of 40 min per FOV per session. Cells were then manually segmented, and single-cell fluorescence traces were extracted by averaging the fluorescence of all pixels masking the soma, using ImageJ (version 2-0-0-rc-69) software. The mean ΔF/F over the full 2 s of each stimulus condition was used to calculate orientation tuning curves, with background fluorescence (F) in Δ F/F taken as the value of the trace immediately preceding a condition, averaged over all conditions. The raw calcium traces from cells within individual FOVs (not across FOVs, given different imaging conditions across animals and time points) were sorted by mean fluorescence. Randomly colored ROI view images were created by suite2p (https://www.suite2p.org). For 'tuned' cells in Figure 4 panels F and G, the counts are based on all imaged neurons' individual tuning curves, plotted in MATLAB; any cell showing response to a preferred orientation (including narrowly tuned neurons and broadly tuned neurons) at any temporal frequency (1Hz, 2Hz, 4Hz, 8Hz, or 15Hz) was counted manually as a tuned cell.

RESOURCE AVAILABILITY

All cell counts and statistical analyses are provided in Supplemental Information. The novel plasmids described in this paper have been deposited with Addgene with the accession numbers given in Methods.

SUPPLEMENTAL INFORMATION

Supplemental information can be found online.
A preprint version of this paper is available on bioRxiv.

ACKNOWLEDGMENTS

We thank Tanya Daigle and Hongkui Zeng for sharing the Ai63 mouse line, Jacque Ip, Chloe Delepine, and Mriganka Sur for sharing mice, Chang Liu for assistance with optimizing MATLAB code for analysis of the functional imaging data, and Sara Beach for helpful suggestions on the manuscript. Research reported in this publication was supported by BRAIN Initiative awards RF1MH120017, U01MH106018, U01MH114829, and U19MH114830 from the National Institute of Mental Health.

AUTHOR CONTRIBUTIONS

L.J., N.E.L., M.M., Y.H., and M.Z. cloned constructs; H.A.S. produced viruses with assistance from L.J. and M.Z.; H.A.S. conducted cell culture assays and immunocytochemistry; L.J., N.E.L., and T.K.L. performed surgeries; L.J. and M.Z. performed histology and confocal imaging; L.J. performed two-photon imaging; L.J., M.Z., T.K.L., and N.E.L. managed mouse breeding; I.W. planned and supervised all work; I.W. and L.J. wrote the manuscript with input from the other authors.

DECLARATION OF INTERESTS

I.R.W. is a consultant for Monosynaptix, LLC, advising on design of neuroscientific experiments.

REFERENCES

Albertini, A.A., Ruigrok, R.W., and Blondel, D. (2011). Rabies virus transcription and replication. Advances in virus research *79*, 1-22.

Alitto, H.J., and Usrey, W.M. (2003). Corticothalamic feedback and sensory processing. Curr Opin Neurobiol *13*, 440-445.

Bragg, E.M., Fairless, E.A., Liu, S., and Briggs, F. (2017). Morphology of visual sector thalamic reticular neurons in the macaque monkey suggests retinotopically specialized, parallel stream-mixed input to the lateral geniculate nucleus. J Comp Neurol *525*, 1273-1290.

Briggs, F., Kiley, C.W., Callaway, E.M., and Usrey, W.M. (2016). Morphological Substrates for Parallel Streams of Corticogeniculate Feedback Originating in Both V1 and V2 of the Macaque Monkey. Neuron *90*, 388-399.

Chatterjee, S., Sullivan, H.A., MacLennan, B.J., Xu, R., Hou, Y., Lavin, T.K., Lea, N.E., Michalski, J.E., Babcock, K.R., Dietrich, S.*, et al.* (2018). Nontoxic, double-deletion-mutant rabies viral vectors for retrograde targeting of projection neurons. Nat Neurosci *21*, 638-646.

Chen, T.W., Wardill, T.J., Sun, Y., Pulver, S.R., Renninger, S.L., Baohan, A., Schreiter, E.R., Kerr, R.A., Orger, M.B., Jayaraman, V.*, et al.* (2013). Ultrasensitive fluorescent proteins for imaging neuronal activity. Nature *499*, 295-300.

Connolly, J.D., Hashemi-Nezhad, M., and Lyon, D.C. (2012). Parallel feedback pathways in visual cortex of cats revealed through a modified rabies virus. J Comp Neurol *520*, 988-1004.

Cruz, A.M., Kim, T.H., and Smith, R.J. (2021). Monosynaptic Retrograde Tracing From Prelimbic Neuron Subpopulations Projecting to Either Nucleus Accumbens Core or Rostromedial Tegmental Nucleus. Front Neural Circuits *15*, 639733.

Daigle, T.L., Madisen, L., Hage, T.A., Valley, M.T., Knoblich, U., Larsen, R.S., Takeno, M.M., Huang, L., Gu, H., Larsen, R.*, et al.* (2018). A Suite of Transgenic Driver and Reporter Mouse Lines with Enhanced Brain-Cell-Type Targeting and Functionality. Cell *174*, 465-480 e422.

Dohaku, R., Yamaguchi, M., Yamamoto, N., Shimizu, T., Osakada, F., and Hibi, M. (2019). Tracing of Afferent Connections in the Zebrafish Cerebellum Using Recombinant Rabies Virus. Front Neural Circuits *13*, 30.

Faulkner, R.L., Wall, N.R., Callaway, E.M., and Cline, H.T. (2021). Application of Recombinant Rabies Virus to Xenopus Tadpole Brain. eNeuro.

Finke, S., and Conzelmann, K.K. (2005). Replication strategies of rabies virus. Virus Res.

Foster, N.N., Barry, J., Korobkova, L., Garcia, L., Gao, L., Becerra, M., Sherafat, Y., Peng, B., Li, X., Choi, J.H.*, et al.* (2021). The mouse cortico-basal ganglia-thalamic network. Nature *598*, 188-194.

Gallardo, H.F., Tan, C., and Sadelain, M. (1997). The internal ribosomal entry site of the encephalomyocarditis virus enables reliable coexpression of two transgenes in human primary T lymphocytes. Gene Ther *4*, 1115-1119.

Gomme, E.A., Faul, E.J., Flomenberg, P., McGettigan, J.P., and Schnell, M.J. (2010). Characterization of a single-cycle rabies virus-based vaccine vector. Journal of virology *84*, 2820-2831.

Hasse, J.M., Bragg, E.M., Murphy, A.J., and Briggs, F. (2019). Morphological heterogeneity among corticogeniculate neurons in ferrets: quantification and comparison with a previous report in macaque monkeys. J Comp Neurol *527*, 546-557.

Hidaka, Y., Lim, C.K., Takayama-Ito, M., Park, C.H., Kimitsuki, K., Shiwa, N., Inoue, K.I., and Itou, T. (2018). Segmentation of the rabies virus genome. Virus Res *252*, 68-75.

Horwitz, J.A., Jenni, S., Harrison, S.C., and Whelan, S.P.J. (2020). Structure of a rabies virus polymerase complex from electron cryo-microscopy. Proc Natl Acad Sci U S A *117*, 2099-2107.

Jin, L., Matsuyama, M., Sullivan, H.A., Zhu, M., Lavin, T.K., Hou, Y., Lea, N.E., Pruner, M.T., Ferdínez, M.L.D., and Wickersham, I.R. (2021a). Rabies virus with a destabilization domain added to its nucleoprotein spreads between neurons only if the domain is removed. bioRxiv, 550640.

Jin, L., Sullivan, H.A., Zhu, M., Lavin, T.K., Matsuyama, M., Lea, N.E., Xu, R., Hou, Y., Rutigliani, L., Pruner, M.*, et al.* (2021b). Long-term labeling and imaging of synaptically-connected neuronal networks in vivo using nontoxic, double-deletion-mutant rabies viruses. bioRxiv, 2021.2012.2004.471186.

Koresawa, Y., Miyagawa, S., Ikawa, M., Matsunami, K., Yamada, M., Shirakura, R., and Okabe, M. (2000). Synthesis of a new Cre recombinase gene based on optimal codon usage for mammalian systems. J Biochem *127*, 367-372.

Lavin, T.K., Jin, L., and Wickersham, I.R. (2019). Monosynaptic tracing: a step-by-step protocol. J Chem Neuroanat, 101661.

Liu, K., Kim, J., Kim, D.W., Zhang, Y.S., Bao, H., Denaxa, M., Lim, S.A., Kim, E., Liu, C., Wickersham, I.R., *et al.* (2017). Lhx6-positive GABA-releasing neurons of the zona incerta promote sleep. Nature *548*, 582-587.

Liu, Y.J., Ehrengruber, M.U., Negwer, M., Shao, H.J., Cetin, A.H., and Lyon, D.C. (2013). Tracing inputs to inhibitory or excitatory neurons of mouse and cat visual cortex with a targeted rabies virus. Curr Biol *23*, 1746-1755.

Lyon, D.C., Nassi, J.J., and Callaway, E.M. (2010). A disynaptic relay from superior colliculus to dorsal stream visual cortex in macaque monkey. Neuron *65*, 270-279.

Madisen, L., Garner, A.R., Shimaoka, D., Chuong, A.S., Klapoetke, N.C., Li, L., van der Bourg, A., Niino, Y., Egolf, L., Monetti, C., *et al.* (2015). Transgenic mice for intersectional targeting of neural sensors and effectors with high specificity and performance. Neuron *85*, 942-958.

Madisen, L., Zwingman, T.A., Sunkin, S.M., Oh, S.W., Zariwala, H.A., Gu, H., Ng, L.L., Palmiter, R.D., Hawrylycz, M.J., Jones, A.R., *et al.* (2010). A robust and high-throughput Cre reporting and characterization system for the whole mouse brain. Nature neuroscience *13*, 133-140.

Miyamichi, K., Amat, F., Moussavi, F., Wang, C., Wickersham, I., Wall, N.R., Taniguchi, H., Tasic, B., Huang, Z.J., He, Z., *et al.* (2011). Cortical representations of olfactory input by trans-synaptic tracing. Nature *472*, 191-196.

Morin, B., Kranzusch, P.J., Rahmeh, A.A., and Whelan, S.P. (2013). The polymerase of negative-stranded RNA viruses. Current opinion in virology *3*, 103-110.

Nakagawa, K., Kobayashi, Y., Ito, N., Suzuki, Y., Okada, K., Makino, M., Goto, H., Takahashi, T., and Sugiyama, M. (2017). Molecular Function Analysis of Rabies Virus RNA Polymerase L Protein by Using an L Gene-Deficient Virus. J Virol *91*.

Nassi, J.J., and Callaway, E.M. (2006). Multiple circuits relaying primate parallel visual pathways to the middle temporal area. J Neurosci *26*, 12789-12798.

Nassi, J.J., and Callaway, E.M. (2007). Specialized circuits from primary visual cortex to V2 and area MT. Neuron *55*, 799-808.

Nassi, J.J., Lyon, D.C., and Callaway, E.M. (2006). The parvocellular LGN provides a robust disynaptic input to the visual motion area MT. Neuron *50*, 319-327.

Ogino, T., and Green, T.J. (2019). Transcriptional Control and mRNA Capping by the GDP Polyribonucleotidyltransferase Domain of the Rabies Virus Large Protein. Viruses *11*.

Raymond, C.S., and Soriano, P. (2007). High-efficiency FLP and PhiC31 site-specific recombination in mammalian cells. PLoS One *2*, e162.

Reardon, T.R., Murray, A.J., Turi, G.F., Wirblich, C., Croce, K.R., Schnell, M.J., Jessell, T.M., and Losonczy, A. (2016). Rabies Virus CVS-N2c(DeltaG) Strain Enhances Retrograde Synaptic Transfer and Neuronal Viability. Neuron *89*, 711-724.

Ren, W., Centeno, M.V., Wei, X., Wickersham, I., Martina, M., Apkarian, A.V., and Surmeier, D.J. (2021). Adaptive alterations in the mesoaccumbal network after peripheral nerve injury. Pain *162*, 895-906.

Rockland, K.S. (2021). A Closer Look at Corticothalamic "Loops". Front Neural Circuits *15*, 632668.

Rouiller, E.M., and Welker, E. (2000). A comparative analysis of the morphology of corticothalamic projections in mammals. Brain Res Bull *53*, 727-741.

Roy, D.S., Zhang, Y., Aida, T., Choi, S., Chen, Q., Hou, Y., Lea, N.E., Skaggs, K.M., Quay, J.C., Liew, M., *et al.* (2021). Anterior thalamic dysfunction underlies cognitive deficits in a subset of neuropsychiatric disease models. Neuron *109*, 2590-2603 e2513.

Satou, C., Neve, R.L., Oyibo, H.K., Zmarz, P., Huang, K.-H., Bouldoires, E.A., Mori, T., Higashijima, S.-i., Keller, G.B., and Friedrich, R.W. (2021). A viral toolbox for conditional and transneuronal gene expression in zebrafish. bioRxiv, 2021.2003.2025.436574.

Schwarz, L.A., Miyamichi, K., Gao, X.J., Beier, K.T., Weissbourd, B., DeLoach, K.E., Ren, J., Ibanes, S., Malenka, R.C., Kremer, E.J., *et al.* (2015). Viral-genetic tracing of the input-output organization of a central noradrenaline circuit. Nature.

Shaner, N.C., Campbell, R.E., Steinbach, P.A., Giepmans, B.N., Palmer, A.E., and Tsien, R.Y. (2004). Improved monomeric red, orange and yellow fluorescent proteins derived from Discosoma sp. red fluorescent protein. Nat Biotechnol *22*, 1567-1572.

Siu, C., Balsor, J., Merlin, S., Federer, F., and Angelucci, A. (2021). A direct interareal feedback-to-feedforward circuit in primate visual cortex. Nat Commun *12*, 4911.

Smith, M.L., Asada, N., and Malenka, R.C. (2021). Anterior cingulate inputs to nucleus accumbens control the social transfer of pain and analgesia. Science *371*, 153-159.

Stephenson-Jones, M., Yu, K., Ahrens, S., Tucciarone, J.M., van Huijstee, A.N., Mejia, L.A., Penzo, M.A., Tai, L.H., Wilbrecht, L., and Li, B. (2016). A basal ganglia circuit for evaluating action outcomes. Nature *539*, 289-293.

Tallquist, M.D., and Soriano, P. (2000). Epiblast-restricted Cre expression in MORE mice: a tool to distinguish embryonic vs. extra-embryonic gene function. Genesis *26*, 113-115.

Tasic, B., Yao, Z., Graybuck, L.T., Smith, K.A., Nguyen, T.N., Bertagnolli, D., Goldy, J., Garren, E., Economo, M.N., Viswanathan, S.*, et al.* (2018). Shared and distinct transcriptomic cell types across neocortical areas. Nature *563*, 72-78.

Te Velthuis, A.J.W., Grimes, J.M., and Fodor, E. (2021). Structural insights into RNA polymerases of negative-sense RNA viruses. Nat Rev Microbiol *19*, 303-318.

Wall, N.R., Wickersham, I.R., Cetin, A., De La Parra, M., and Callaway, E.M. (2010). Monosynaptic circuit tracing in vivo through Cre-dependent targeting and complementation of modified rabies virus. P Natl Acad Sci USA.

Wang, G.P., and Bushman, F.D. (2006). A statistical method for comparing viral growth curves. J Virol Methods *135*, 118-123.

Wang, L., Sharma, K., Deng, H.X., Siddique, T., Grisotti, G., Liu, E., and Roos, R.P. (2008). Restricted expression of mutant SOD1 in spinal motor neurons and interneurons induces motor neuron pathology. Neurobiol Dis *29*, 400-408.

Wickersham, I.R., Finke, S., Conzelmann, K.K., and Callaway, E.M. (2007a). Retrograde neuronal tracing with a deletion-mutant rabies virus. Nature Methods *4*, 47-49.

Wickersham, I.R., Lyon, D.C., Barnard, R.J., Mori, T., Finke, S., Conzelmann, K.K., Young, J.A., and Callaway, E.M. (2007b). Monosynaptic restriction of transsynaptic tracing from single, genetically targeted neurons. Neuron *53*, 639-647.

Wickersham, I.R., and Sullivan, H.A. (2015). Rabies viral vectors for monosynaptic tracing and targeted transgene expression in neurons. Cold Spring Harb Protoc *2015*, 375-385.

Wickersham, I.R., Sullivan, H.A., and Seung, H.S. (2010). Production of glycoprotein-deleted rabies viruses for monosynaptic tracing and high-level gene expression in neurons. Nature protocols *5*, 595-606.

Wu, X., Morishita, W., Beier, K.T., Heifets, B.D., and Malenka, R.C. (2021). 5-HT modulation of a medial septal circuit tunes social memory stability. Nature *599*, 96-101.

Yao, S., Wang, Q., Hirokawa, K.E., Ouellette, B., Ahmed, R., Bomben, J., Brouner, K., Casal, L., Caldejon, S., Cho, A.*, et al.* (2021). A whole-brain monosynaptic input connectome to neuron classes in mouse visual cortex. bioRxiv, 2021.2009.2029.459010.

Yarch, J., Federer, F., and Angelucci, A. (2017). Local Circuits of V1 Layer 4B Neurons Projecting to V2 Thick Stripes Define Distinct Cell Classes and Avoid Cytochrome Oxidase Blobs. J Neurosci *37*, 422-436.

Zhu, P., Narita, Y., Bundschuh, S.T., Fajardo, O., Scharer, Y.P., Chattopadhyaya, B., Bouldoires, E.A., Stepien, A.E., Deisseroth, K., Arber, S.*, et al.* (2009). Optogenetic Dissection of Neuronal Circuits in Zebrafish using Viral Gene Transfer and the Tet System. Front Neural Circuits *3*, 21.

FIGURES

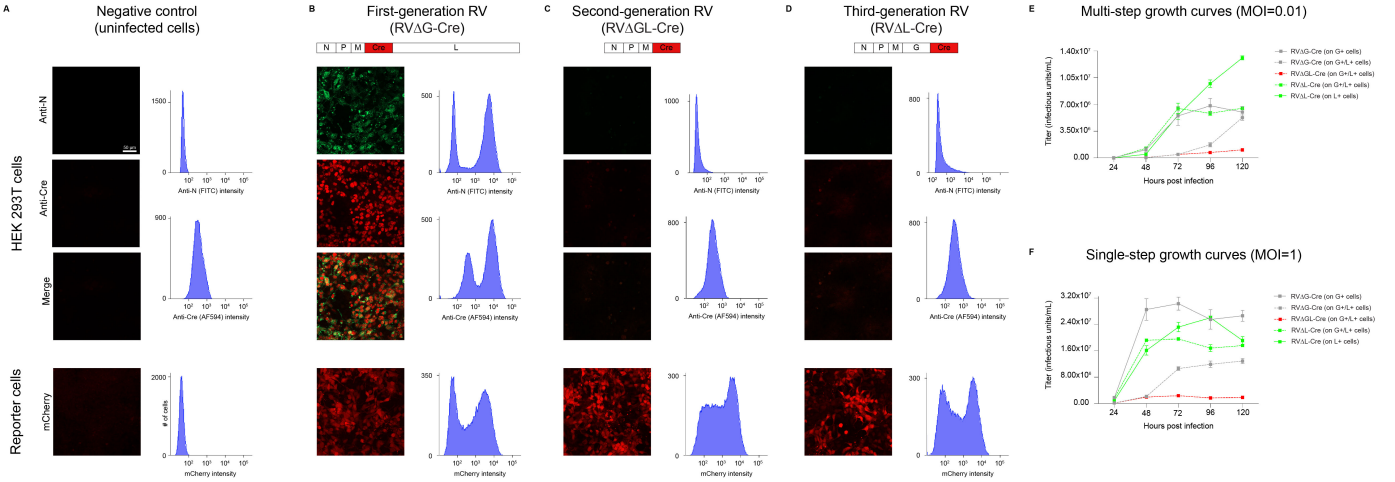

Figure 1. Rabies virus with just the polymerase gene deleted (ΔL) is phenotypically similar to double-deletion-mutant (ΔGL) virus but replicates to much higher titers within complementing cells.
(A-D) Deletion of just the polymerase gene L reduces transgene expression to levels that are very low but still sufficient to support reporter allele recombination in Cre reporter cells.
(A) Negative controls (uninfected cells). Top: Uninfected HEK 293T cells stained for rabies virus nucleoprotein (green) and for Cre (red). Histograms to right of panels show flow cytometric quantification of baseline fluorescence of uninfected cells in these channels. Bottom: Uninfected reporter cells which express mCherry following Cre recombination. Little signal is seen in these negative controls.
(B) Cells infected with a first-generation (ΔG) vector expressing Cre. Both Cre and N are expressed at very high levels, and infected Cre reporter cells brightly express mCherry (note that dilutions at which roughly half of cells were infected were chosen for this figure).
(C) Consistent with our previous findings (Chatterjee et al., 2018), expression of both nucleoprotein and Cre from a second-generation (ΔGL) vector is drastically reduced with respect to the first-generation vector, with expression levels comparable to those seen in negative controls. Despite this, the low Cre levels are still high enough to activate mCherry expression in reporter cells.
(D) A third-generation (ΔL) vector expresses nucleoprotein and Cre at similarly very low levels, but again Cre expression is nonetheless high enough to successfully activate mCherry expression in reporter cells.
(E-F) Third-generation (ΔL) vectors grow to much high titers in cultured cells than second-generation (ΔGL) ones do.
(E) Viral titers in supernatants of complementing cells (expressing L, G, or both) infected with ΔL, ΔGL, or ΔG viruses at a multiplicity of infection (MOI) of 0.01 ("multi-step growth curves"), with supernatants collected every 24 hours for five days. Whereas a ΔGL virus only achieves 1.05E+06 infectious units (i.u.)/ml over the duration of the experiment, the ΔL virus grows to 6.2-fold higher on the same cell line, and 12.5-fold higher on a line expressing L alone. The highest ΔL titers obtained in this experiment were significantly higher than the highest obtained with a first-generation (ΔG) virus (single-factor ANOVA, p = 3.24E-03, n = 3 replicates per condition).
(F) Similarly, at a MOI of 1 ("single-step" growth curves), the ΔGL virus titer peaks at 2.37E+06 i.u./ml, whereas the peak titer of the ΔL virus is 2.60E+07 i.u./ml, 11.0-fold higher than that of the ΔGL virus and not significantly different from that of the ΔG virus (single-factor ANOVA, p = 0.105, n = 3 replicates per condition). Graphs in (E-F) show means ± s.e.m.

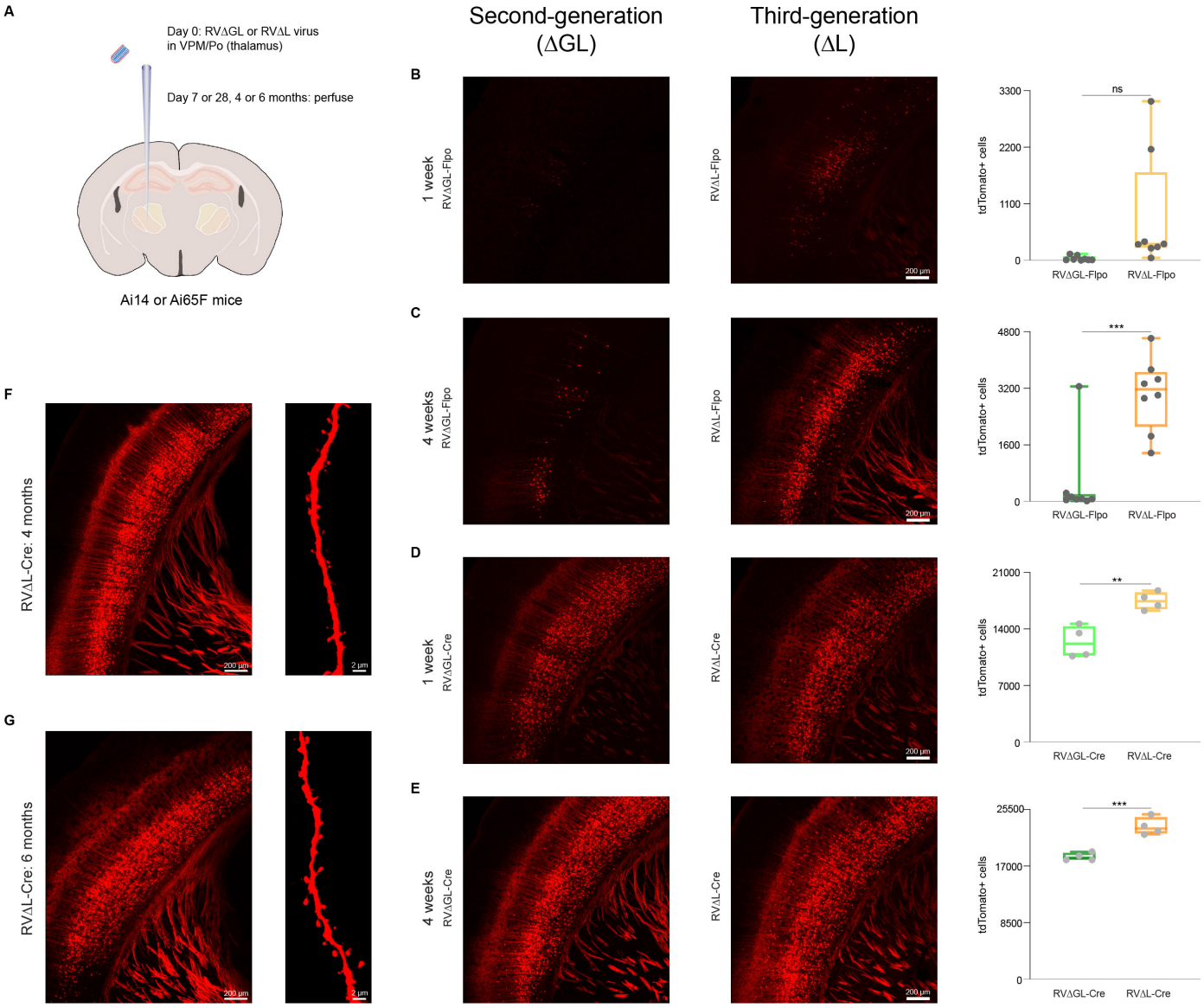

Figure 2. Third-generation (ΔL) rabies viral vectors retrogradely label many more projection neurons *in vivo* than do second-generation (ΔGL) ones and leave cells morphologically normal for at least six months.

(A) Design of experiments retrogradely targeting corticothalamic cells in reporter mice. Either second-generation vector RVΔGL-Flpo or RVΔGL-Cre, or third-generation vector RVΔL-Flpo or RVΔL-Cre, was injected into somatosensory thalamus (VPM/Po) of either Ai65F (Flpo reporter) or Ai14 (Cre reporter). Mice were perfused 1 week (b, d), 4 weeks (c, e), 4 months (f), or 6 months later (g).

(B-E) Efficacy comparison of Flpo- and Cre-expressing ΔGL and ΔL vectors.

(B) Corticothalamic neurons in S1 of Ai65F mice labeled with RVΔGL-Flpo (left) or RVΔL-Flpo (center) at 1 week postinjection. Scale bar: 200 µm, applies to both images. Counts of labeled cortical neurons are shown at right (each data point is the total number in one series consisting of every sixth 50 µm section from a given brain - see Methods). The ΔL virus labeled 24 times as many cortical neurons than the ΔGL virus did, although the difference in this case is not significant due to high variance (single-factor ANOVA, p = 0.0608, n = 8 mice per group).

(C) Corticothalamic neurons in S1 of Ai65F mice labeled with RVΔGL-Flpo (left) or RVΔL-Flpo (center) at 4 weeks postinjection. Scale bar: 200 µm, applies to both images. Counts of labeled cortical neurons are shown at right. The ΔL virus labeled 6.25 times as many cortical neurons than the ΔGL virus did, an extremely significant difference (single-factor ANOVA, p = 0.000321, n = 8 mice per group).

(D) Corticothalamic neurons in S1 of Ai14 mice labeled with RVΔGL-Cre (left) or RVΔL-Cre (center) at 1 week postinjection. Scale bar: 200 µm, applies to both images. Counts of labeled cortical neurons are

shown at right. The ΔL virus labeled 1.4 times as many cortical neurons than the ΔGL virus did, a highly significant difference (single-factor ANOVA, p = 0.00420, n = 8 mice per group).
(E) Corticothalamic neurons in S1 of Ai14 mice labeled with RVΔGL-Cre (left) or RVΔL-Cre (center) at 4 weeks postinjection. Scale bar: 200 μm, applies to both images. Counts of labeled cortical neurons are shown at right. The ΔL virus labeled 1.25 times as many cortical neurons than the ΔGL virus did, an extremely significant difference (single-factor ANOVA, p = 0.000738, n = 8 mice each group).
(F) Corticothalamic neurons in S1 of Ai14 mice labeled with RVΔL-Cre at 4 months postinjection. Cells appear morphologically completely normal, with no blebbing or decomposition of processes. Scale bars: 200 μm (left image) and 2 μm (right image).
(G) Corticothalamic neurons in S1 of Ai14 mice labeled with RVΔL-Cre at 6 months postinjection. Cells still appear morphologically completely normal. Scale bars: 200 μm (left image) and 2 μm (right image).

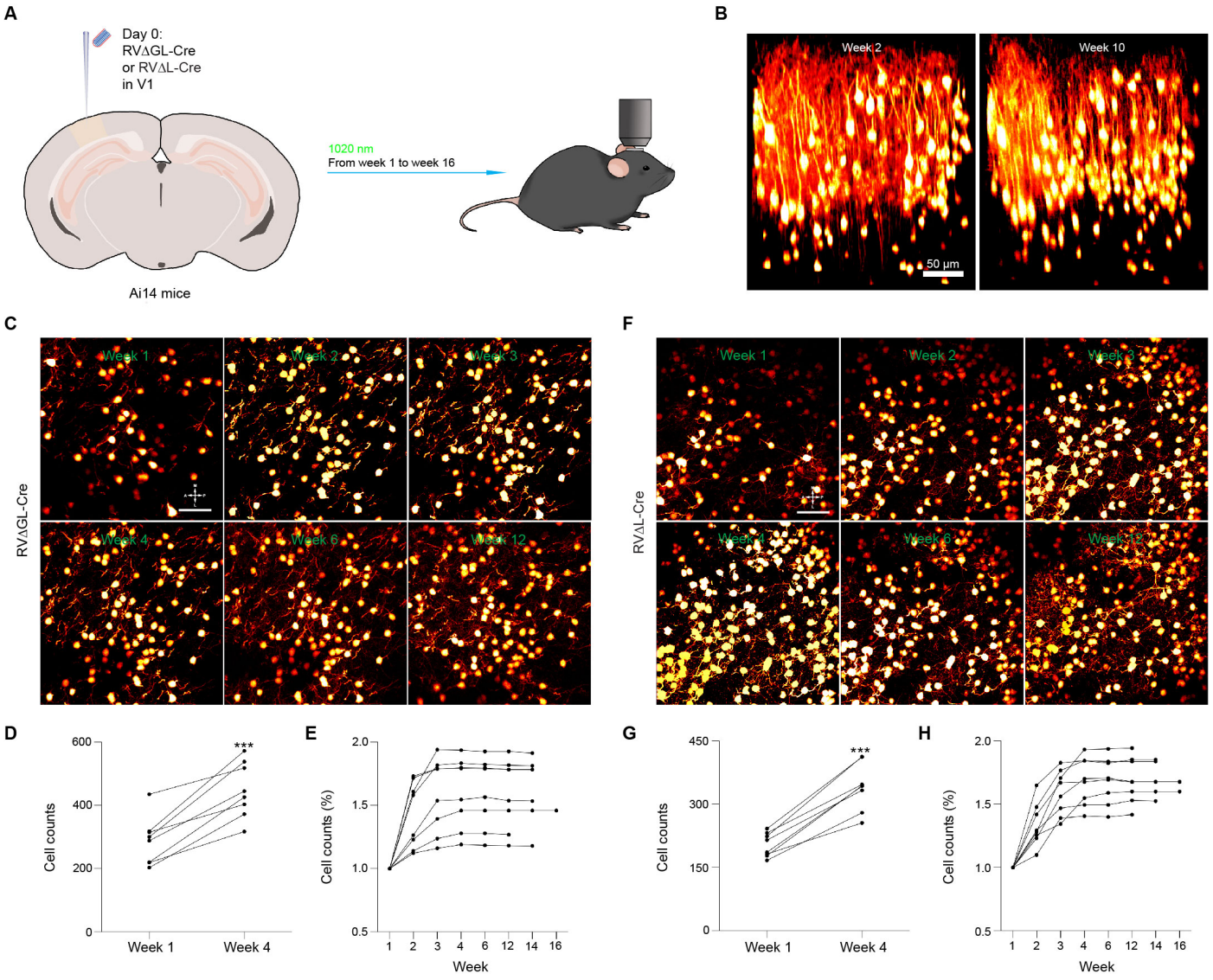

Figure 3. Neurons labeled by ΔL rabies virus survive for at least 16 weeks.

(A) Experimental design for longitudinal structural two-photon imaging *in vivo*. Second-generation (ΔGL) or third-generation (ΔL) virus expressing Cre was injected in primary visual cortex of reporter mice, then the injection sites were imaged repeatedly for the following 16 weeks.

(B) Example renderings of the same volume of cortex labeled by RVΔL-Cre and imaged with a two-photon microscope at two different timepoints, 2 weeks (left) and 10 weeks (right). Every labeled neuron visible at 2 weeks is still present at 10 weeks. Scale bar: 50 μm. See also Video S1.

(C) & (F), Example two-photon images of single fields of view (FOV) of cortex labeled by either the second-generation vector RVΔGL-Cre (C) or the third-generation vector RVΔL-Cre (F), imaged at different timepoints, from 1 week (top left) to 12 weeks (bottom right). All labeled neurons visible at earlier timepoints are still present at later ones, for both viruses. Scale bars: 50 μm, apply to all images.

(D) & (G), Absolute numbers of cells visibly labeled by RVΔGL-Cre (D) or RVΔL-Cre (G) for all structural FOVs in the study, at the 1-week and 4-week timepoints. Numbers of visibly labeled cells increased by 56.27% for ΔGL and by 67.77% for ΔL, as we found previously for second-generation vectors (Chatterjee et al., 2018)), suggesting accumulation and persistent activity of recombinase on this timescale. These increases were both extremely significant (one-tailed paired t-tests, p = 0.000132 (ΔGL) and 0.00001003 (ΔL), n = 8 FOVs each virus), but there was no significant difference between the increases seen for the two viruses (two-tailed unpaired t-test, p = 0.5187, n = 8 FOVs per group).

(E) & (H), Percentages of cells visibly labeled by RVΔGL-Cre (E) and RVΔL-Cre (H) over time, relative to the numbers visible at 1 week after rabies injection; each connected set of dots represents numbers seen in a given FOV at the different time points. For both viruses, the numbers of labeled neurons remain nearly

740 constant from the 4-week timepoint onward, as we found previously (Chatterjee et al., 2018) for ΔGL virus.
741 Imaging was discontinued for some mice at weeks 12 or 14 due to cloudiness of the optical windows.

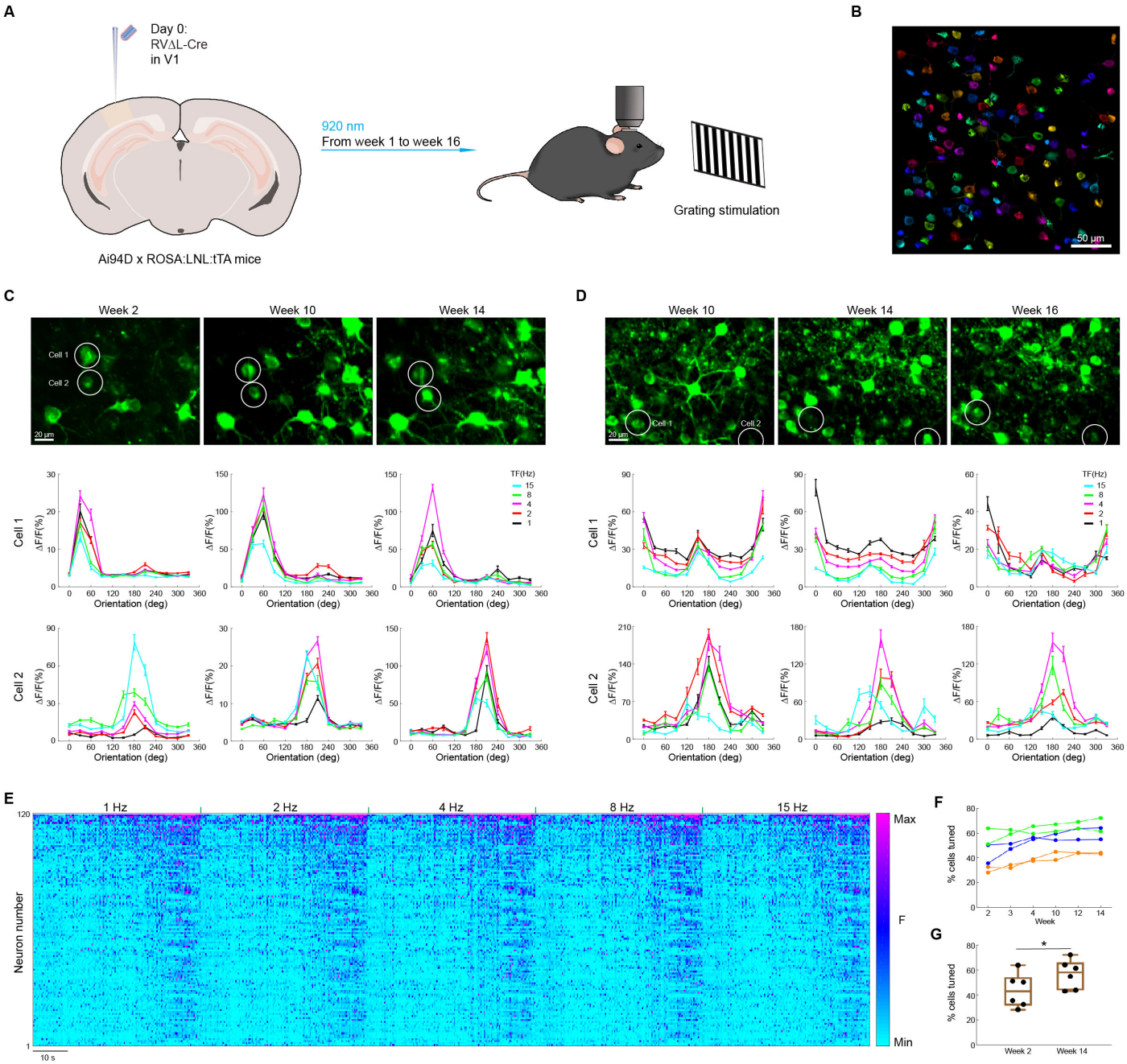

Figure 4. ΔL rabies virus does not appear to perturb neurons' visual response properties for at least 16 weeks.

(A) Experimental design for longitudinal functional two-photon imaging *in vivo*. ΔL virus expressing Cre was injected in primary visual cortex of reporter mice expressing GCaMP6s (Chen et al., 2013) after Cre recombination, then the injection sites were imaged while the awake mice were presented with drifting grating stimuli of different orientations and temporal frequencies, repeatedly for 16 weeks following virus injection.

(B) Example FOV from a GCaMP6s imaging session 16 weeks after RV injection. Individual analyzed cells are randomly pseudocolored. This is the same FOV as shown in Video S2. Scale bar: 50 μm.

(C-D) Long-term stability of orientation and temporal frequency tuning in RVΔL-Cre-labeled neurons. The top rows show maximum intensity projections of the imaged GCaMP6s signal in two different FOVs at three different timepoints for each FOV. Scale bars: 20 μm, apply to all images. Visual response tuning curves of the two circled cells in each FOV at the corresponding timepoint, obtained with drifting gratings presented at 12 directions of motion and 5 temporal frequencies (TF) (mean ΔF/F ± s.e.m., averaged over 10 repeats), are shown under each image. More examples from the same FOV are shown in Figure S5.

(E) Single-cell fluorescence time courses for 120 cells at the 12-week timepoint, showing activity over all five temporal frequencies (mean ΔF/F, averaged over 10 repeats). Cells are ranked in descending order of total activity. Scale bar: 10 s.
(F) Percentages of labeled cells that were visually tuned (see Methods), from 6 different FOVs in 3 mice imaged over 14 weeks. Connected sets of dots in a given color indicate data from a single mouse (data from 2 FOVs are shown per mouse).
(G) Comparison of the percentages of labeled cells that were visually tuned at 2 weeks and 14 weeks. The percentages increased moderately but significantly between the two timepoints, from 60% to 68% (paired two-sample t-test, $p = 0.0178$, $n = 6$).

SUPPLEMENTAL INFORMATION

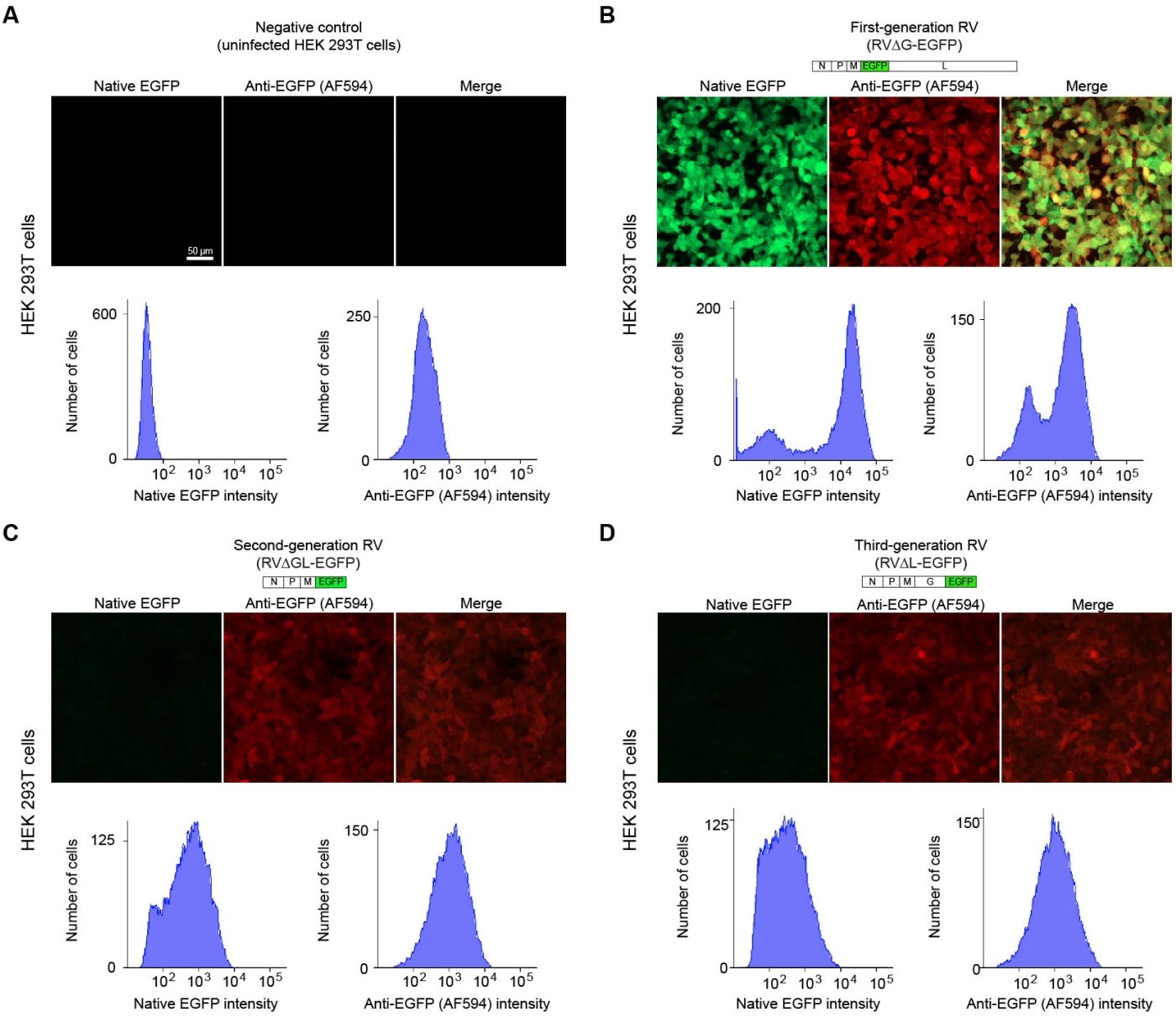

Figure S1. ΔL and ΔGL viruses express EGFP at similarly low levels, Related to Figure 1
Confocal images and flow cytometric histograms showing native and immunostained EGFP signal in uninfected cells (A) and cells infected with first-generation (ΔG) virus (B), second-generation (ΔGL) virus (C), or third-generation virus (D) expressing EGFP. Scale bar: 50 µm, applies to all images.

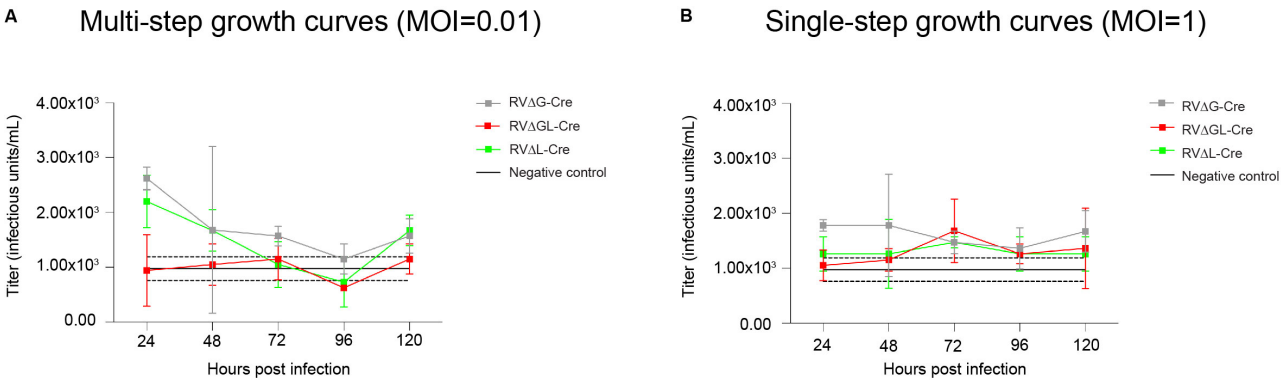

Figure S2. ΔG, ΔGL, and ΔL viruses do not propagate in non-complementing cells, Related to Figure 1

Viral titers in supernatants of BHK-21 cells not expressing any rabies viral genes, infected with ΔL, ΔGL, or ΔG viruses at a multiplicity of infection (MOI) of 0.01 ("multi-step growth curves", panel A) or 1 ("single-step" growth curves, panel B), with supernatants collected every 24 hours for five days. Graphs show mean ± s.e.m. .Black lines show negative control "titers" calculated from uninfected reporter cells (mean ± s.e.m. of 10 samples). Note that the titers in these graphs are 3-4 orders of magnitude lower than those obtained on complementing cells (Figure 1).

File S1. Titers and statistics for growth dynamics experiments, Related to Figure 1

See following pages.

FACS data from Single-step growth curves (Infectious units/mL)	24hr	48hr	72hr	96hr	120hr
(1) RVΔGL-Cre (on B19L-G_01 cells)	1.89E+05	1.99E+06	2.39E+06	1.76E+06	1.94E+06
(2) RVΔGL-Cre (on B19L-G_01 cells)	1.48E+05	1.97E+06	2.46E+06	1.77E+06	1.92E+06
(3) RVΔGL-Cre (on B19L-G_01 cells)	1.55E+05	1.89E+06	2.25E+06	1.55E+06	1.73E+06
(7) RVΔL-Cre (on B19L_02 cells)	8.60E+05	1.84E+07	2.60E+07	2.71E+07	2.10E+07
(8) RVΔL-Cre (on B19L_02 cells)	7.05E+05	1.35E+07	2.11E+07	2.54E+07	1.92E+07
(9) RVΔL-Cre (on B19L_02 cells)	1.17E+06	1.65E+07	2.25E+07	2.56E+07	1.70E+07
(13) RVΔL-Cre (on B19L-G_01 cells)	1.31E+06	1.92E+07	2.02E+07	1.87E+07	1.79E+07
(14) RVΔL-Cre (on B19L-G_01 cells)	1.88E+06	1.96E+07	1.92E+07	1.67E+07	1.79E+07
(15) RVΔL-Cre (on B19L-G_01 cells)	1.61E+06	1.89E+07	1.94E+07	1.51E+07	1.70E+07
(19) RVΔG-Cre (on B19G3-2 cells)	2.13E+06	3.12E+07	3.22E+07	3.02E+07	2.71E+07
(20) RVΔG-Cre (on B19G3-2 cells)	1.89E+06	3.22E+07	3.24E+07	2.63E+07	2.92E+07
(21) RVΔG-Cre (on B19G3-2 cells)	1.39E+06	2.19E+07	2.64E+07	2.01E+07	2.35E+07
(25) RVΔG-Cre (on B19L-G_01 cells)	1.71E+05	2.04E+06	1.14E+07	1.36E+07	1.37E+07
(26) RVΔG-Cre (on B19L-G_01 cells)	1.84E+05	2.40E+06	1.09E+07	1.18E+07	1.36E+07
(27) RVΔG-Cre (on B19L-G_01 cells)	1.65E+05	2.01E+06	9.61E+06	1.02E+07	1.14E+07

FACS data from Multi-step growth curves (Infectious units/mL)	24hr	48hr	72hr	96hr	120hr
(4) RVΔGL-Cre (on B19L-G_01 cells)	6.22E+03	4.36E+04	5.17E+05	7.09E+05	1.21E+06
(5) RVΔGL-Cre (on B19L-G_01 cells)	7.77E+03	4.39E+04	4.47E+05	7.78E+05	9.81E+05
(6) RVΔGL-Cre (on B19L-G_01 cells)	5.91E+03	6.31E+04	4.30E+05	6.82E+05	9.70E+05
(10) RVΔL-Cre (on B19L_02 cells)	6.84E+03	5.48E+05	5.50E+06	9.25E+06	1.26E+07
(11) RVΔL-Cre (on B19L_02 cells)	5.28E+03	2.96E+05	4.67E+06	9.18E+06	1.34E+07
(12) RVΔL-Cre (on B19L_02 cells)	5.59E+03	6.57E+05	6.63E+06	1.07E+07	1.34E+07
(16) RVΔL-Cre (on B19L-G_01 cells)	8.71E+03	1.31E+06	7.69E+06	5.80E+06	6.84E+06
(17) RVΔL-Cre (on B19L-G_01 cells)	4.04E+03	1.38E+06	6.40E+06	6.33E+06	6.57E+06
(18) RVΔL-Cre (on B19L-G_01 cells)	5.91E+03	1.11E+06	5.39E+06	5.40E+06	6.11E+06
(22) RVΔG-Cre (on B19G3-2 cells)	3.31E+04	1.70E+06	7.96E+06	8.63E+06	7.39E+06
(23) RVΔG-Cre (on B19G3-2 cells)	2.24E+04	6.82E+05	4.13E+06	5.36E+06	4.99E+06
(24) RVΔG-Cre (on B19G3-2 cells)	2.43E+04	8.56E+05	4.41E+06	6.52E+06	5.61E+06
(28) RVΔG-Cre (on B19L-G_01 cells)	6.84E+03	6.25E+04	5.56E+05	2.23E+06	5.91E+06
(29) RVΔG-Cre (on B19L-G_01 cells)	5.28E+03	3.23E+04	3.33E+05	1.27E+06	4.70E+06
(30) RVΔG-Cre (on B19L-G_01 cells)	8.40E+03	4.24E+04	4.88E+05	1.67E+06	5.21E+06

Average titers for Single-step growth curves (Infectious units/mL)	24hr	48hr	72hr	96hr	120hr
(1-3) RVΔGL-Cre (on B19L-G_01 cells)	1.64E+05	1.95E+06	2.37E+06	1.69E+06	1.86E+06
(7-9) RVΔL-Cre (on B19L_02 cells)	9.12E+05	1.61E+07	2.32E+07	2.60E+07	1.91E+07
(13-15) RVΔL-Cre (on B19L-G_01 cells)	1.60E+06	1.92E+07	**1.96E+07**	1.68E+07	1.76E+07
(19-21) RVΔG-Cre (on B19G3-2 cells)	1.81E+06	2.85E+07	3.03E+07	2.55E+07	2.66E+07
(25-27) RVΔG-Cre (on B19L-G_01 cells)	1.73E+05	2.15E+06	1.06E+07	1.19E+07	**1.29E+07**

Standard error of the mean for Single-step growth curves (Infectious units/mL)	24hr	48hr	72hr	96hr	120hr
(1-3) RVΔGL-Cre (on B19L-G_01 cells)	1.27E+04	3.12E+04	6.11E+04	7.25E+04	6.73E+04
(7-9) RVΔL-Cre (on B19L_02 cells)	1.37E+05	1.42E+06	1.45E+06	5.43E+05	1.16E+06
(13-15) RVΔL-Cre (on B19L-G_01 cells)	1.64E+05	2.12E+05	3.21E+05	1.04E+06	3.02E+05
(19-21) RVΔG-Cre (on B19G3-2 cells)	2.18E+05	3.29E+06	1.99E+06	2.94E+06	1.66E+06
(25-27) RVΔG-Cre (on B19L-G_01 cells)	5.71E+03	1.24E+05	5.38E+05	9.85E+05	7.57E+05

Average titers for Multi-step growth curves (Infectious units/mL)	24hr	48hr	72hr	96hr	120hr
(4-6) RVΔGL-Cre (on B19L-G_01 cells)	6.63E+03	5.02E+04	4.65E+05	7.23E+05	1.05E+06
(10-12) RVΔL-Cre (on B19L_02 cells)	5.91E+03	5.00E+05	5.60E+06	9.72E+06	1.31E+07
(16-18) RVΔL-Cre (on B19L-G_01 cells)	6.22E+03	1.27E+06	6.49E+06	5.84E+06	**6.51E+06**
(22-24) RVΔG-Cre (on B19G3-2 cells)	2.66E+04	1.08E+06	5.50E+06	6.83E+06	6.00E+06
(28-30) RVΔG-Cre (on B19L-G_01 cells)	6.84E+03	4.57E+04	4.59E+05	1.72E+06	**5.27E+06**

Standard error of the mean for Multi-step growth curves	24hr	48hr	72hr	96hr	120hr
(4-6) RVΔGL-Cre (on B19L-G_01 cells)	5.78E+02	6.45E+03	2.69E+04	2.87E+04	7.74E+04
(10-12) RVΔL-Cre (on B19L_02 cells)	4.75E+02	1.07E+05	5.70E+05	5.06E+05	2.77E+05
(16-18) RVΔL-Cre (on B19L-G_01 cells)	1.36E+03	8.07E+04	6.63E+05	2.71E+05	2.13E+05
(22-24) RVΔG-Cre (on B19G3-2 cells)	3.28E+03	3.16E+05	1.23E+06	9.57E+05	7.18E+05
(28-30) RVΔG-Cre (on B19L-G_01 cells)	8.98E+02	8.87E+03	6.60E+04	2.80E+05	3.51E+05

Conditions with the highest average titers for Single-step growth curves	Infectious units/mL
(1-3) RVΔGL-Cre (on B19L-G_01 cells): 72hr	2.39E+06
	2.46E+06
	2.25E+06
(7-9) RVΔL-Cre (on B19L_02 cells): 96hr	2.71E+07
	2.54E+07
	2.56E+07
(19-21) RVΔG-Cre (on B19G3-2 cells): 72hr	3.22E+07
	3.24E+07
	2.64E+07

Column1	Column2
average "titer" of BC-FLEX cells:	
3.63E+03	
Individual BC-FLEX negative "titers"	
NEG_01	5.28E+03
NEG_02	5.91E+03
NEG_03	3.11E+03
NEG_04	2.80E+03
NEG_05	2.17E+03
NEG_06	2.49E+03

Conditions with the highest average titers for Multi-step growth curves	Infectious units/mL
(4-6) RVΔGL-Cre (on B19L-G_01 cells): 120hr	1.21E+06
	9.81E+05
	9.70E+05
(10-12) RVΔL-Cre (on B19L_02 cells): 120hr	1.26E+07
	1.34E+07
	1.34E+07
(22-24) RVΔG-Cre (on B19G3-2 cells): 96hr	8.63E+06
	5.36E+06
	6.52E+06

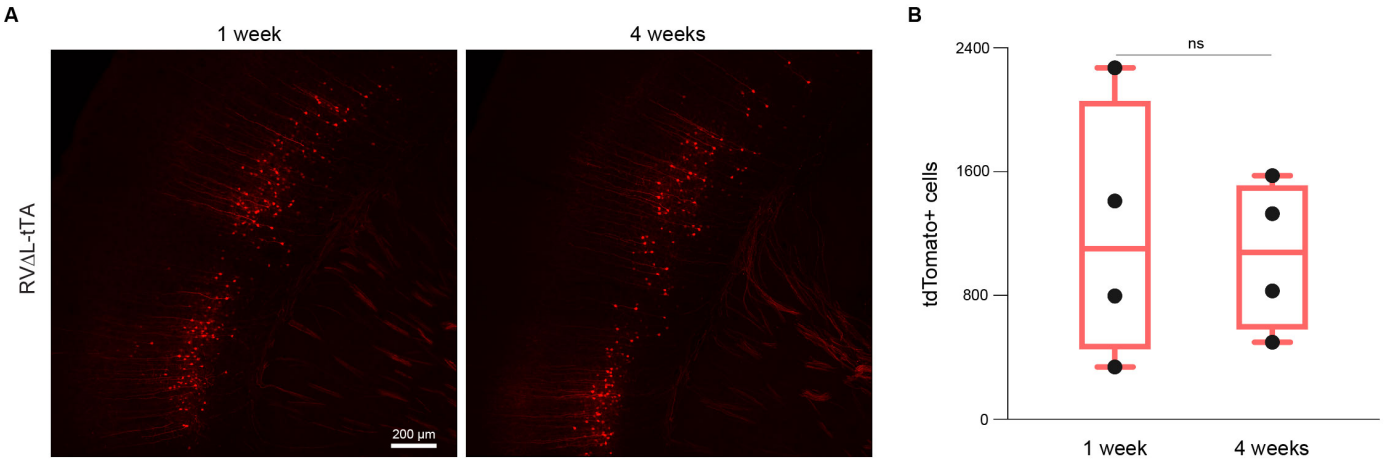

Figure S3. Retrograde targeting with third-generation (ΔL) rabies virus expressing the tetracycline transactivator, Related to Figure 2

(A) Corticothalamic neurons retrogradely labeled by a ΔL virus expressing tTA injected in the somatosensory thalamus of Ai63 reporter mice (Daigle et al., 2018) (tdTomato driven by TRE-tight) 1 week (left image) or 4 weeks (right image) prior to perfusion. Scale bar: 200 µm, applies to both images.
(B) Counts of total labeled cortical neurons across every sixth section (see Methods) of each mouse brain. Numbers are not significantly different between the two time points (single factor ANOVA, $p = 0.772$, $n = 4$ mice per group).

File S2. Cell counts and statistics for retrograde targeting experiments, Related to Figure 2

See following pages.

Condition	Mouse number	Section number	Cell counts
RVΔGL-Flpo: 1 week	21021505LJ	10	5
RVΔGL-Flpo: 1 week	21021505LJ	11	8
RVΔGL-Flpo: 1 week	21021505LJ	12	9
RVΔGL-Flpo: 1 week	21021505LJ	total:	22
RVΔGL-Flpo: 1 week	21021506LJ	9	5
RVΔGL-Flpo: 1 week	21021506LJ	10	6
RVΔGL-Flpo: 1 week	21021506LJ	11	4
RVΔGL-Flpo: 1 week	21021506LJ	12	3
RVΔGL-Flpo: 1 week	21021506LJ	total:	18
RVΔGL-Flpo: 1 week	21021507LJ	5	1
RVΔGL-Flpo: 1 week	21021507LJ	6	27
RVΔGL-Flpo: 1 week	21021507LJ	7	29
RVΔGL-Flpo: 1 week	21021507LJ	8	25
RVΔGL-Flpo: 1 week	21021507LJ	9	20
RVΔGL-Flpo: 1 week	21021507LJ	10	10
RVΔGL-Flpo: 1 week	21021507LJ	11	4
RVΔGL-Flpo: 1 week	21021507LJ	12	3
RVΔGL-Flpo: 1 week	21021507LJ	13	2
RVΔGL-Flpo: 1 week	21021507LJ	total:	121
RVΔGL-Flpo: 1 week	21021508LJ	11	1
RVΔGL-Flpo: 1 week	21021508LJ	15	1
RVΔGL-Flpo: 1 week	21021508LJ	total:	2
RVΔGL-Flpo: 1 week	21052505LJ	9	1
RVΔGL-Flpo: 1 week	21052505LJ	10	5
RVΔGL-Flpo: 1 week	21052505LJ	11	1
RVΔGL-Flpo: 1 week	21052505LJ	total:	7
RVΔGL-Flpo: 1 week	21052506LJ	11	4
RVΔGL-Flpo: 1 week	21052506LJ	12	4
RVΔGL-Flpo: 1 week	21052506LJ	total:	8
RVΔGL-Flpo: 1 week	21052507LJ	6	2
RVΔGL-Flpo: 1 week	21052507LJ	7	20
RVΔGL-Flpo: 1 week	21052507LJ	8	45
RVΔGL-Flpo: 1 week	21052507LJ	9	26
RVΔGL-Flpo: 1 week	21052507LJ	10	5
RVΔGL-Flpo: 1 week	21052507LJ	total:	98
RVΔGL-Flpo: 1 week	21052508LJ	8	1
RVΔGL-Flpo: 1 week	21052508LJ	10	1
RVΔGL-Flpo: 1 week	21052508LJ	11	1
RVΔGL-Flpo: 1 week	21052508LJ	12	1
RVΔGL-Flpo: 1 week	21052508LJ	14	2
RVΔGL-Flpo: 1 week	21052508LJ	total:	6
RVΔL-Flpo: 1 week	21021805LJ	1	57
RVΔL-Flpo: 1 week	21021805LJ	2	20
RVΔL-Flpo: 1 week	21021805LJ	3	11
RVΔL-Flpo: 1 week	21021805LJ	4	115
RVΔL-Flpo: 1 week	21021805LJ	5	270
RVΔL-Flpo: 1 week	21021805LJ	6	399
RVΔL-Flpo: 1 week	21021805LJ	7	428
RVΔL-Flpo: 1 week	21021805LJ	8	542
RVΔL-Flpo: 1 week	21021805LJ	9	416
RVΔL-Flpo: 1 week	21021805LJ	10	368
RVΔL-Flpo: 1 week	21021805LJ	11	240
RVΔL-Flpo: 1 week	21021805LJ	12	106
RVΔL-Flpo: 1 week	21021805LJ	13	42

RVΔL-Flpo: 1 week	21021805LJ	14	52
RVΔL-Flpo: 1 week	21021805LJ	15	27
RVΔL-Flpo: 1 week	21021805LJ	total:	3093
RVΔL-Flpo: 1 week	21021806LJ	1	1
RVΔL-Flpo: 1 week	21021806LJ	4	5
RVΔL-Flpo: 1 week	21021806LJ	5	3
RVΔL-Flpo: 1 week	21021806LJ	6	4
RVΔL-Flpo: 1 week	21021806LJ	7	16
RVΔL-Flpo: 1 week	21021806LJ	8	35
RVΔL-Flpo: 1 week	21021806LJ	9	93
RVΔL-Flpo: 1 week	21021806LJ	10	74
RVΔL-Flpo: 1 week	21021806LJ	11	40
RVΔL-Flpo: 1 week	21021806LJ	12	24
RVΔL-Flpo: 1 week	21021806LJ	13	11
RVΔL-Flpo: 1 week	21021806LJ	14	7
RVΔL-Flpo: 1 week	21021806LJ	15	7
RVΔL-Flpo: 1 week	21021806LJ	total:	320
RVΔL-Flpo: 1 week	21021807LJ	5	1
RVΔL-Flpo: 1 week	21021807LJ	6	2
RVΔL-Flpo: 1 week	21021807LJ	7	6
RVΔL-Flpo: 1 week	21021807LJ	8	8
RVΔL-Flpo: 1 week	21021807LJ	9	35
RVΔL-Flpo: 1 week	21021807LJ	10	64
RVΔL-Flpo: 1 week	21021807LJ	11	80
RVΔL-Flpo: 1 week	21021807LJ	12	55
RVΔL-Flpo: 1 week	21021807LJ	13	34
RVΔL-Flpo: 1 week	21021807LJ	14	13
RVΔL-Flpo: 1 week	21021807LJ	15	13
RVΔL-Flpo: 1 week	21021807LJ	total:	311
RVΔL-Flpo: 1 week	21021808LJ	6	7
RVΔL-Flpo: 1 week	21021808LJ	7	13
RVΔL-Flpo: 1 week	21021808LJ	8	48
RVΔL-Flpo: 1 week	21021808LJ	9	74
RVΔL-Flpo: 1 week	21021808LJ	10	57
RVΔL-Flpo: 1 week	21021808LJ	11	20
RVΔL-Flpo: 1 week	21021808LJ	12	13
RVΔL-Flpo: 1 week	21021808LJ	13	13
RVΔL-Flpo: 1 week	21021808LJ	14	14
RVΔL-Flpo: 1 week	21021808LJ	15	4
RVΔL-Flpo: 1 week	21021808LJ	total:	263
RVΔL-Flpo: 1 week	21052607LJ	4	3
RVΔL-Flpo: 1 week	21052607LJ	5	2
RVΔL-Flpo: 1 week	21052607LJ	6	4
RVΔL-Flpo: 1 week	21052607LJ	7	11
RVΔL-Flpo: 1 week	21052607LJ	8	10
RVΔL-Flpo: 1 week	21052607LJ	9	4
RVΔL-Flpo: 1 week	21052607LJ	11	6
RVΔL-Flpo: 1 week	21052607LJ	12	7
RVΔL-Flpo: 1 week	21052607LJ	total:	47
RVΔL-Flpo: 1 week	21052608LJ	1	105
RVΔL-Flpo: 1 week	21052608LJ	2	116
RVΔL-Flpo: 1 week	21052608LJ	3	110
RVΔL-Flpo: 1 week	21052608LJ	4	192
RVΔL-Flpo: 1 week	21052608LJ	5	395
RVΔL-Flpo: 1 week	21052608LJ	6	389

RVΔL-Flpo: 1 week	21052608LJ	7	421
RVΔL-Flpo: 1 week	21052608LJ	8	340
RVΔL-Flpo: 1 week	21052608LJ	9	72
RVΔL-Flpo: 1 week	21052608LJ	10	14
RVΔL-Flpo: 1 week	21052608LJ	11	5
RVΔL-Flpo: 1 week	21052608LJ	12	2
RVΔL-Flpo: 1 week	21052608LJ	total:	2161
RVΔL-Flpo: 1 week	21060302LJ	1	8
RVΔL-Flpo: 1 week	21060302LJ	2	10
RVΔL-Flpo: 1 week	21060302LJ	3	17
RVΔL-Flpo: 1 week	21060302LJ	4	24
RVΔL-Flpo: 1 week	21060302LJ	5	22
RVΔL-Flpo: 1 week	21060302LJ	6	29
RVΔL-Flpo: 1 week	21060302LJ	7	34
RVΔL-Flpo: 1 week	21060302LJ	8	59
RVΔL-Flpo: 1 week	21060302LJ	9	78
RVΔL-Flpo: 1 week	21060302LJ	10	46
RVΔL-Flpo: 1 week	21060302LJ	11	16
RVΔL-Flpo: 1 week	21060302LJ	12	12
RVΔL-Flpo: 1 week	21060302LJ	13	6
RVΔL-Flpo: 1 week	21060302LJ	14	2
RVΔL-Flpo: 1 week	21060302LJ	15	2
RVΔL-Flpo: 1 week	21060302LJ	total:	365
RVΔL-Flpo: 1 week	21060303LJ	1	7
RVΔL-Flpo: 1 week	21060303LJ	2	9
RVΔL-Flpo: 1 week	21060303LJ	3	10
RVΔL-Flpo: 1 week	21060303LJ	4	16
RVΔL-Flpo: 1 week	21060303LJ	5	22
RVΔL-Flpo: 1 week	21060303LJ	6	27
RVΔL-Flpo: 1 week	21060303LJ	7	25
RVΔL-Flpo: 1 week	21060303LJ	8	27
RVΔL-Flpo: 1 week	21060303LJ	9	36
RVΔL-Flpo: 1 week	21060303LJ	10	30
RVΔL-Flpo: 1 week	21060303LJ	11	15
RVΔL-Flpo: 1 week	21060303LJ	12	7
RVΔL-Flpo: 1 week	21060303LJ	14	6
RVΔL-Flpo: 1 week	21060303LJ	15	1
RVΔL-Flpo: 1 week	21060303LJ	total:	238
RVΔGL-Flpo: 4 weeks	21021501LJ	7	2
RVΔGL-Flpo: 4 weeks	21021501LJ	8	12
RVΔGL-Flpo: 4 weeks	21021501LJ	9	25
RVΔGL-Flpo: 4 weeks	21021501LJ	10	26
RVΔGL-Flpo: 4 weeks	21021501LJ	11	7
RVΔGL-Flpo: 4 weeks	21021501LJ	12	3
RVΔGL-Flpo: 4 weeks	21021501LJ	13	3
RVΔGL-Flpo: 4 weeks	21021501LJ	14	1
RVΔGL-Flpo: 4 weeks	21021501LJ	15	1
RVΔGL-Flpo: 4 weeks	21021501LJ	total:	80
RVΔGL-Flpo: 4 weeks	21021502LJ	9	2
RVΔGL-Flpo: 4 weeks	21021502LJ	10	25
RVΔGL-Flpo: 4 weeks	21021502LJ	11	26
RVΔGL-Flpo: 4 weeks	21021502LJ	12	5
RVΔGL-Flpo: 4 weeks	21021502LJ	13	4
RVΔGL-Flpo: 4 weeks	21021502LJ	total:	62
RVΔGL-Flpo: 4 weeks	21021503LJ	1	88

RVΔGL-Flpo: 4 weeks	21021503LJ	2	129
RVΔGL-Flpo: 4 weeks	21021503LJ	3	199
RVΔGL-Flpo: 4 weeks	21021503LJ	4	254
RVΔGL-Flpo: 4 weeks	21021503LJ	5	312
RVΔGL-Flpo: 4 weeks	21021503LJ	6	396
RVΔGL-Flpo: 4 weeks	21021503LJ	7	351
RVΔGL-Flpo: 4 weeks	21021503LJ	8	391
RVΔGL-Flpo: 4 weeks	21021503LJ	9	359
RVΔGL-Flpo: 4 weeks	21021503LJ	10	295
RVΔGL-Flpo: 4 weeks	21021503LJ	11	133
RVΔGL-Flpo: 4 weeks	21021503LJ	12	216
RVΔGL-Flpo: 4 weeks	21021503LJ	13	59
RVΔGL-Flpo: 4 weeks	21021503LJ	14	40
RVΔGL-Flpo: 4 weeks	21021503LJ	15	32
RVΔGL-Flpo: 4 weeks	21021503LJ	total:	3254
RVΔGL-Flpo: 4 weeks	21021504LJ	3	1
RVΔGL-Flpo: 4 weeks	21021504LJ	4	4
RVΔGL-Flpo: 4 weeks	21021504LJ	5	22
RVΔGL-Flpo: 4 weeks	21021504LJ	6	24
RVΔGL-Flpo: 4 weeks	21021504LJ	7	56
RVΔGL-Flpo: 4 weeks	21021504LJ	8	78
RVΔGL-Flpo: 4 weeks	21021504LJ	9	32
RVΔGL-Flpo: 4 weeks	21021504LJ	10	18
RVΔGL-Flpo: 4 weeks	21021504LJ	11	1
RVΔGL-Flpo: 4 weeks	21021504LJ	12	1
RVΔGL-Flpo: 4 weeks	21021504LJ	total:	237
RVΔGL-Flpo: 4 weeks	21052501LJ	2	1
RVΔGL-Flpo: 4 weeks	21052501LJ	4	1
RVΔGL-Flpo: 4 weeks	21052501LJ	7	2
RVΔGL-Flpo: 4 weeks	21052501LJ	8	6
RVΔGL-Flpo: 4 weeks	21052501LJ	9	9
RVΔGL-Flpo: 4 weeks	21052501LJ	10	9
RVΔGL-Flpo: 4 weeks	21052501LJ	11	2
RVΔGL-Flpo: 4 weeks	21052501LJ	12	6
RVΔGL-Flpo: 4 weeks	21052501LJ	13	4
RVΔGL-Flpo: 4 weeks	21052501LJ	14	1
RVΔGL-Flpo: 4 weeks	21052501LJ	15	2
RVΔGL-Flpo: 4 weeks	21052501LJ	total:	43
RVΔGL-Flpo: 4 weeks	21052502LJ	6	2
RVΔGL-Flpo: 4 weeks	21052502LJ	7	1
RVΔGL-Flpo: 4 weeks	21052502LJ	8	4
RVΔGL-Flpo: 4 weeks	21052502LJ	11	1
RVΔGL-Flpo: 4 weeks	21052502LJ	14	3
RVΔGL-Flpo: 4 weeks	21052502LJ	15	3
RVΔGL-Flpo: 4 weeks	21052502LJ	total:	14
RVΔGL-Flpo: 4 weeks	21052503LJ	6	2
RVΔGL-Flpo: 4 weeks	21052503LJ	8	1
RVΔGL-Flpo: 4 weeks	21052503LJ	9	9
RVΔGL-Flpo: 4 weeks	21052503LJ	10	45
RVΔGL-Flpo: 4 weeks	21052503LJ	11	33
RVΔGL-Flpo: 4 weeks	21052503LJ	12	17
RVΔGL-Flpo: 4 weeks	21052503LJ	13	10
RVΔGL-Flpo: 4 weeks	21052503LJ	14	7
RVΔGL-Flpo: 4 weeks	21052503LJ	15	6
RVΔGL-Flpo: 4 weeks	21052503LJ	total:	130

RVΔGL-Flpo: 4 weeks	21052504LJ	7	2
RVΔGL-Flpo: 4 weeks	21052504LJ	8	13
RVΔGL-Flpo: 4 weeks	21052504LJ	9	18
RVΔGL-Flpo: 4 weeks	21052504LJ	10	16
RVΔGL-Flpo: 4 weeks	21052504LJ	11	8
RVΔGL-Flpo: 4 weeks	21052504LJ	12	3
RVΔGL-Flpo: 4 weeks	21052504LJ	13	3
RVΔGL-Flpo: 4 weeks	21052504LJ	14	1
RVΔGL-Flpo: 4 weeks	21052504LJ	15	1
RVΔGL-Flpo: 4 weeks	21052504LJ	total:	65
RVΔL-Flpo: 4 weeks	21021801LJ	1	36
RVΔL-Flpo: 4 weeks	21021801LJ	2	18
RVΔL-Flpo: 4 weeks	21021801LJ	3	2
RVΔL-Flpo: 4 weeks	21021801LJ	4	28
RVΔL-Flpo: 4 weeks	21021801LJ	5	180
RVΔL-Flpo: 4 weeks	21021801LJ	6	415
RVΔL-Flpo: 4 weeks	21021801LJ	7	622
RVΔL-Flpo: 4 weeks	21021801LJ	8	649
RVΔL-Flpo: 4 weeks	21021801LJ	9	739
RVΔL-Flpo: 4 weeks	21021801LJ	10	577
RVΔL-Flpo: 4 weeks	21021801LJ	11	431
RVΔL-Flpo: 4 weeks	21021801LJ	12	211
RVΔL-Flpo: 4 weeks	21021801LJ	13	166
RVΔL-Flpo: 4 weeks	21021801LJ	14	170
RVΔL-Flpo: 4 weeks	21021801LJ	15	370
RVΔL-Flpo: 4 weeks	21021801LJ	total:	4614
RVΔL-Flpo: 4 weeks	21021802LJ	1	3
RVΔL-Flpo: 4 weeks	21021802LJ	2	6
RVΔL-Flpo: 4 weeks	21021802LJ	3	8
RVΔL-Flpo: 4 weeks	21021802LJ	5	32
RVΔL-Flpo: 4 weeks	21021802LJ	6	224
RVΔL-Flpo: 4 weeks	21021802LJ	7	279
RVΔL-Flpo: 4 weeks	21021802LJ	8	287
RVΔL-Flpo: 4 weeks	21021802LJ	9	457
RVΔL-Flpo: 4 weeks	21021802LJ	10	501
RVΔL-Flpo: 4 weeks	21021802LJ	11	491
RVΔL-Flpo: 4 weeks	21021802LJ	12	211
RVΔL-Flpo: 4 weeks	21021802LJ	13	287
RVΔL-Flpo: 4 weeks	21021802LJ	14	220
RVΔL-Flpo: 4 weeks	21021802LJ	total:	3006
RVΔL-Flpo: 4 weeks	21021803LJ	2	6
RVΔL-Flpo: 4 weeks	21021803LJ	3	9
RVΔL-Flpo: 4 weeks	21021803LJ	4	48
RVΔL-Flpo: 4 weeks	21021803LJ	5	177
RVΔL-Flpo: 4 weeks	21021803LJ	6	247
RVΔL-Flpo: 4 weeks	21021803LJ	7	339
RVΔL-Flpo: 4 weeks	21021803LJ	8	316
RVΔL-Flpo: 4 weeks	21021803LJ	9	322
RVΔL-Flpo: 4 weeks	21021803LJ	10	205
RVΔL-Flpo: 4 weeks	21021803LJ	11	78
RVΔL-Flpo: 4 weeks	21021803LJ	12	46
RVΔL-Flpo: 4 weeks	21021803LJ	13	41
RVΔL-Flpo: 4 weeks	21021803LJ	14	13
RVΔL-Flpo: 4 weeks	21021803LJ	total:	1847
RVΔL-Flpo: 4 weeks	21021804LJ	1	6

RVΔL-Flpo: 4 weeks	21021804LJ	2	14
RVΔL-Flpo: 4 weeks	21021804LJ	3	2
RVΔL-Flpo: 4 weeks	21021804LJ	4	57
RVΔL-Flpo: 4 weeks	21021804LJ	5	359
RVΔL-Flpo: 4 weeks	21021804LJ	6	414
RVΔL-Flpo: 4 weeks	21021804LJ	7	469
RVΔL-Flpo: 4 weeks	21021804LJ	8	576
RVΔL-Flpo: 4 weeks	21021804LJ	9	533
RVΔL-Flpo: 4 weeks	21021804LJ	10	383
RVΔL-Flpo: 4 weeks	21021804LJ	11	283
RVΔL-Flpo: 4 weeks	21021804LJ	12	114
RVΔL-Flpo: 4 weeks	21021804LJ	13	34
RVΔL-Flpo: 4 weeks	21021804LJ	14	87
RVΔL-Flpo: 4 weeks	21021804LJ	total:	3331
RVΔL-Flpo: 4 weeks	21052601LJ	2	1
RVΔL-Flpo: 4 weeks	21052601LJ	3	1
RVΔL-Flpo: 4 weeks	21052601LJ	5	16
RVΔL-Flpo: 4 weeks	21052601LJ	6	10
RVΔL-Flpo: 4 weeks	21052601LJ	7	28
RVΔL-Flpo: 4 weeks	21052601LJ	8	92
RVΔL-Flpo: 4 weeks	21052601LJ	9	161
RVΔL-Flpo: 4 weeks	21052601LJ	10	232
RVΔL-Flpo: 4 weeks	21052601LJ	11	280
RVΔL-Flpo: 4 weeks	21052601LJ	12	201
RVΔL-Flpo: 4 weeks	21052601LJ	13	143
RVΔL-Flpo: 4 weeks	21052601LJ	14	106
RVΔL-Flpo: 4 weeks	21052601LJ	15	98
RVΔL-Flpo: 4 weeks	21052601LJ	total:	1369
RVΔL-Flpo: 4 weeks	21052602LJ	1	49
RVΔL-Flpo: 4 weeks	21052602LJ	2	12
RVΔL-Flpo: 4 weeks	21052602LJ	3	17
RVΔL-Flpo: 4 weeks	21052602LJ	4	51
RVΔL-Flpo: 4 weeks	21052602LJ	5	163
RVΔL-Flpo: 4 weeks	21052602LJ	6	418
RVΔL-Flpo: 4 weeks	21052602LJ	7	489
RVΔL-Flpo: 4 weeks	21052602LJ	8	526
RVΔL-Flpo: 4 weeks	21052602LJ	9	510
RVΔL-Flpo: 4 weeks	21052602LJ	10	319
RVΔL-Flpo: 4 weeks	21052602LJ	11	179
RVΔL-Flpo: 4 weeks	21052602LJ	12	72
RVΔL-Flpo: 4 weeks	21052602LJ	13	48
RVΔL-Flpo: 4 weeks	21052602LJ	14	32
RVΔL-Flpo: 4 weeks	21052602LJ	15	34
RVΔL-Flpo: 4 weeks	21052602LJ	total:	2919
RVΔL-Flpo: 4 weeks	21052603LJ	1	38
RVΔL-Flpo: 4 weeks	21052603LJ	2	33
RVΔL-Flpo: 4 weeks	21052603LJ	3	16
RVΔL-Flpo: 4 weeks	21052603LJ	4	44
RVΔL-Flpo: 4 weeks	21052603LJ	5	302
RVΔL-Flpo: 4 weeks	21052603LJ	6	648
RVΔL-Flpo: 4 weeks	21052603LJ	7	636
RVΔL-Flpo: 4 weeks	21052603LJ	8	666
RVΔL-Flpo: 4 weeks	21052603LJ	9	582
RVΔL-Flpo: 4 weeks	21052603LJ	10	409
RVΔL-Flpo: 4 weeks	21052603LJ	11	207

RVΔL-Flpo: 4 weeks	21052603LJ	12	79
RVΔL-Flpo: 4 weeks	21052603LJ	13	26
RVΔL-Flpo: 4 weeks	21052603LJ	14	25
RVΔL-Flpo: 4 weeks	21052603LJ	15	19
RVΔL-Flpo: 4 weeks	21052603LJ	total:	3730
RVΔL-Flpo: 4 weeks	21052606LJ	1	43
RVΔL-Flpo: 4 weeks	21052606LJ	2	23
RVΔL-Flpo: 4 weeks	21052606LJ	3	14
RVΔL-Flpo: 4 weeks	21052606LJ	4	32
RVΔL-Flpo: 4 weeks	21052606LJ	5	220
RVΔL-Flpo: 4 weeks	21052606LJ	6	503
RVΔL-Flpo: 4 weeks	21052606LJ	7	616
RVΔL-Flpo: 4 weeks	21052606LJ	8	622
RVΔL-Flpo: 4 weeks	21052606LJ	9	560
RVΔL-Flpo: 4 weeks	21052606LJ	10	403
RVΔL-Flpo: 4 weeks	21052606LJ	11	179
RVΔL-Flpo: 4 weeks	21052606LJ	12	82
RVΔL-Flpo: 4 weeks	21052606LJ	13	56
RVΔL-Flpo: 4 weeks	21052606LJ	14	68
RVΔL-Flpo: 4 weeks	21052606LJ	15	33
RVΔL-Flpo: 4 weeks	21052606LJ	total:	3454
RVΔGL-Cre: 1 week	21021703LJ	1	422
RVΔGL-Cre: 1 week	21021703LJ	2	395
RVΔGL-Cre: 1 week	21021703LJ	3	606
RVΔGL-Cre: 1 week	21021703LJ	4	543
RVΔGL-Cre: 1 week	21021703LJ	5	637
RVΔGL-Cre: 1 week	21021703LJ	6	848
RVΔGL-Cre: 1 week	21021703LJ	7	1145
RVΔGL-Cre: 1 week	21021703LJ	8	1183
RVΔGL-Cre: 1 week	21021703LJ	9	1292
RVΔGL-Cre: 1 week	21021703LJ	10	1311
RVΔGL-Cre: 1 week	21021703LJ	11	1377
RVΔGL-Cre: 1 week	21021703LJ	12	1251
RVΔGL-Cre: 1 week	21021703LJ	13	998
RVΔGL-Cre: 1 week	21021703LJ	14	835
RVΔGL-Cre: 1 week	21021703LJ	15	641
RVΔGL-Cre: 1 week	21021703LJ	total:	13484
RVΔGL-Cre: 1 week	21021704LJ	1	918
RVΔGL-Cre: 1 week	21021704LJ	2	975
RVΔGL-Cre: 1 week	21021704LJ	3	1144
RVΔGL-Cre: 1 week	21021704LJ	4	1404
RVΔGL-Cre: 1 week	21021704LJ	5	1491
RVΔGL-Cre: 1 week	21021704LJ	6	1377
RVΔGL-Cre: 1 week	21021704LJ	7	1231
RVΔGL-Cre: 1 week	21021704LJ	8	1337
RVΔGL-Cre: 1 week	21021704LJ	9	1135
RVΔGL-Cre: 1 week	21021704LJ	10	1058
RVΔGL-Cre: 1 week	21021704LJ	11	711
RVΔGL-Cre: 1 week	21021704LJ	12	568
RVΔGL-Cre: 1 week	21021704LJ	13	443
RVΔGL-Cre: 1 week	21021704LJ	14	432
RVΔGL-Cre: 1 week	21021704LJ	15	411
RVΔGL-Cre: 1 week	21021704LJ	total:	14635
RVΔGL-Cre: 1 week	21021707LJ	1	497
RVΔGL-Cre: 1 week	21021707LJ	2	568

RVΔGL-Cre: 1 week	21021707LJ	3	454
RVΔGL-Cre: 1 week	21021707LJ	4	454
RVΔGL-Cre: 1 week	21021707LJ	5	583
RVΔGL-Cre: 1 week	21021707LJ	6	873
RVΔGL-Cre: 1 week	21021707LJ	7	973
RVΔGL-Cre: 1 week	21021707LJ	8	1133
RVΔGL-Cre: 1 week	21021707LJ	9	1220
RVΔGL-Cre: 1 week	21021707LJ	10	1176
RVΔGL-Cre: 1 week	21021707LJ	11	994
RVΔGL-Cre: 1 week	21021707LJ	12	645
RVΔGL-Cre: 1 week	21021707LJ	13	467
RVΔGL-Cre: 1 week	21021707LJ	14	330
RVΔGL-Cre: 1 week	21021707LJ	15	280
RVΔGL-Cre: 1 week	21021707LJ	total:	10647
RVΔGL-Cre: 1 week	21021708LJ	1	271
RVΔGL-Cre: 1 week	21021708LJ	2	303
RVΔGL-Cre: 1 week	21021708LJ	3	386
RVΔGL-Cre: 1 week	21021708LJ	4	634
RVΔGL-Cre: 1 week	21021708LJ	5	805
RVΔGL-Cre: 1 week	21021708LJ	6	931
RVΔGL-Cre: 1 week	21021708LJ	7	1029
RVΔGL-Cre: 1 week	21021708LJ	8	1186
RVΔGL-Cre: 1 week	21021708LJ	9	1227
RVΔGL-Cre: 1 week	21021708LJ	10	1102
RVΔGL-Cre: 1 week	21021708LJ	11	1019
RVΔGL-Cre: 1 week	21021708LJ	12	666
RVΔGL-Cre: 1 week	21021708LJ	13	431
RVΔGL-Cre: 1 week	21021708LJ	14	369
RVΔGL-Cre: 1 week	21021708LJ	15	486
RVΔGL-Cre: 1 week	21021708LJ	total:	10845
RVΔL-Cre: 1 week	21021905LJ	1	1161
RVΔL-Cre: 1 week	21021905LJ	2	1093
RVΔL-Cre: 1 week	21021905LJ	3	1072
RVΔL-Cre: 1 week	21021905LJ	4	1079
RVΔL-Cre: 1 week	21021905LJ	5	1318
RVΔL-Cre: 1 week	21021905LJ	6	1417
RVΔL-Cre: 1 week	21021905LJ	7	1541
RVΔL-Cre: 1 week	21021905LJ	8	1510
RVΔL-Cre: 1 week	21021905LJ	9	1500
RVΔL-Cre: 1 week	21021905LJ	10	1549
RVΔL-Cre: 1 week	21021905LJ	11	1381
RVΔL-Cre: 1 week	21021905LJ	12	1109
RVΔL-Cre: 1 week	21021905LJ	13	532
RVΔL-Cre: 1 week	21021905LJ	14	380
RVΔL-Cre: 1 week	21021905LJ	15	265
RVΔL-Cre: 1 week	21021905LJ	total:	16907
RVΔL-Cre: 1 week	21021906LJ	1	985
RVΔL-Cre: 1 week	21021906LJ	2	1012
RVΔL-Cre: 1 week	21021906LJ	3	1020
RVΔL-Cre: 1 week	21021906LJ	4	1060
RVΔL-Cre: 1 week	21021906LJ	5	1082
RVΔL-Cre: 1 week	21021906LJ	6	1515
RVΔL-Cre: 1 week	21021906LJ	7	1808
RVΔL-Cre: 1 week	21021906LJ	8	1675
RVΔL-Cre: 1 week	21021906LJ	9	1538

RVΔL-Cre: 1 week	21021906LJ	10	1728
RVΔL-Cre: 1 week	21021906LJ	11	955
RVΔL-Cre: 1 week	21021906LJ	12	1018
RVΔL-Cre: 1 week	21021906LJ	13	993
RVΔL-Cre: 1 week	21021906LJ	14	701
RVΔL-Cre: 1 week	21021906LJ	15	483
RVΔL-Cre: 1 week	21021906LJ	16	350
RVΔL-Cre: 1 week	21021906LJ	total:	17923
RVΔL-Cre: 1 week	21021907LJ	1	1207
RVΔL-Cre: 1 week	21021907LJ	2	1083
RVΔL-Cre: 1 week	21021907LJ	3	1152
RVΔL-Cre: 1 week	21021907LJ	4	1225
RVΔL-Cre: 1 week	21021907LJ	5	1336
RVΔL-Cre: 1 week	21021907LJ	6	1558
RVΔL-Cre: 1 week	21021907LJ	7	1498
RVΔL-Cre: 1 week	21021907LJ	8	1709
RVΔL-Cre: 1 week	21021907LJ	9	1547
RVΔL-Cre: 1 week	21021907LJ	10	1718
RVΔL-Cre: 1 week	21021907LJ	11	1503
RVΔL-Cre: 1 week	21021907LJ	12	1249
RVΔL-Cre: 1 week	21021907LJ	13	845
RVΔL-Cre: 1 week	21021907LJ	14	626
RVΔL-Cre: 1 week	21021907LJ	15	495
RVΔL-Cre: 1 week	21021907LJ	total:	18751
RVΔL-Cre: 1 week	21021908LJ	1	1011
RVΔL-Cre: 1 week	21021908LJ	2	892
RVΔL-Cre: 1 week	21021908LJ	3	896
RVΔL-Cre: 1 week	21021908LJ	4	957
RVΔL-Cre: 1 week	21021908LJ	5	1243
RVΔL-Cre: 1 week	21021908LJ	6	1448
RVΔL-Cre: 1 week	21021908LJ	7	1568
RVΔL-Cre: 1 week	21021908LJ	8	1459
RVΔL-Cre: 1 week	21021908LJ	9	1573
RVΔL-Cre: 1 week	21021908LJ	10	1313
RVΔL-Cre: 1 week	21021908LJ	11	1146
RVΔL-Cre: 1 week	21021908LJ	12	1046
RVΔL-Cre: 1 week	21021908LJ	13	774
RVΔL-Cre: 1 week	21021908LJ	14	483
RVΔL-Cre: 1 week	21021908LJ	15	448
RVΔL-Cre: 1 week	21021908LJ	total:	16257
RVΔGL-Cre: 4 weeks	21021701LJ	1	1314
RVΔGL-Cre: 4 weeks	21021701LJ	2	1246
RVΔGL-Cre: 4 weeks	21021701LJ	3	1351
RVΔGL-Cre: 4 weeks	21021701LJ	4	1601
RVΔGL-Cre: 4 weeks	21021701LJ	5	1668
RVΔGL-Cre: 4 weeks	21021701LJ	6	1618
RVΔGL-Cre: 4 weeks	21021701LJ	7	1593
RVΔGL-Cre: 4 weeks	21021701LJ	8	1757
RVΔGL-Cre: 4 weeks	21021701LJ	9	1730
RVΔGL-Cre: 4 weeks	21021701LJ	10	1600
RVΔGL-Cre: 4 weeks	21021701LJ	11	1268
RVΔGL-Cre: 4 weeks	21021701LJ	12	931
RVΔGL-Cre: 4 weeks	21021701LJ	13	652
RVΔGL-Cre: 4 weeks	21021701LJ	14	491
RVΔGL-Cre: 4 weeks	21021701LJ	15	336

RVΔGL-Cre: 4 weeks	21021701LJ	total:	19156
RVΔGL-Cre: 4 weeks	21021702LJ	1	957
RVΔGL-Cre: 4 weeks	21021702LJ	2	1175
RVΔGL-Cre: 4 weeks	21021702LJ	3	1414
RVΔGL-Cre: 4 weeks	21021702LJ	4	1470
RVΔGL-Cre: 4 weeks	21021702LJ	5	1481
RVΔGL-Cre: 4 weeks	21021702LJ	6	1654
RVΔGL-Cre: 4 weeks	21021702LJ	7	1616
RVΔGL-Cre: 4 weeks	21021702LJ	8	1601
RVΔGL-Cre: 4 weeks	21021702LJ	9	1717
RVΔGL-Cre: 4 weeks	21021702LJ	10	1449
RVΔGL-Cre: 4 weeks	21021702LJ	11	1132
RVΔGL-Cre: 4 weeks	21021702LJ	12	871
RVΔGL-Cre: 4 weeks	21021702LJ	13	587
RVΔGL-Cre: 4 weeks	21021702LJ	14	456
RVΔGL-Cre: 4 weeks	21021702LJ	15	355
RVΔGL-Cre: 4 weeks	21021702LJ	total:	17935
RVΔGL-Cre: 4 weeks	21021705LJ	1	892
RVΔGL-Cre: 4 weeks	21021705LJ	2	824
RVΔGL-Cre: 4 weeks	21021705LJ	3	879
RVΔGL-Cre: 4 weeks	21021705LJ	4	1094
RVΔGL-Cre: 4 weeks	21021705LJ	5	1182
RVΔGL-Cre: 4 weeks	21021705LJ	6	1318
RVΔGL-Cre: 4 weeks	21021705LJ	7	1482
RVΔGL-Cre: 4 weeks	21021705LJ	8	1637
RVΔGL-Cre: 4 weeks	21021705LJ	9	1666
RVΔGL-Cre: 4 weeks	21021705LJ	10	1796
RVΔGL-Cre: 4 weeks	21021705LJ	11	1636
RVΔGL-Cre: 4 weeks	21021705LJ	12	1415
RVΔGL-Cre: 4 weeks	21021705LJ	13	1121
RVΔGL-Cre: 4 weeks	21021705LJ	14	894
RVΔGL-Cre: 4 weeks	21021705LJ	15	703
RVΔGL-Cre: 4 weeks	21021705LJ	total:	18539
RVΔGL-Cre: 4 weeks	21021706LJ	1	756
RVΔGL-Cre: 4 weeks	21021706LJ	2	817
RVΔGL-Cre: 4 weeks	21021706LJ	3	750
RVΔGL-Cre: 4 weeks	21021706LJ	4	798
RVΔGL-Cre: 4 weeks	21021706LJ	5	920
RVΔGL-Cre: 4 weeks	21021706LJ	6	1337
RVΔGL-Cre: 4 weeks	21021706LJ	7	1485
RVΔGL-Cre: 4 weeks	21021706LJ	8	1490
RVΔGL-Cre: 4 weeks	21021706LJ	9	1641
RVΔGL-Cre: 4 weeks	21021706LJ	10	2004
RVΔGL-Cre: 4 weeks	21021706LJ	11	1955
RVΔGL-Cre: 4 weeks	21021706LJ	12	1453
RVΔGL-Cre: 4 weeks	21021706LJ	13	1122
RVΔGL-Cre: 4 weeks	21021706LJ	14	769
RVΔGL-Cre: 4 weeks	21021706LJ	15	641
RVΔGL-Cre: 4 weeks	21021706LJ	total:	17938
RVΔL-Cre: 4 weeks	21021901LJ	1	943
RVΔL-Cre: 4 weeks	21021901LJ	2	1003
RVΔL-Cre: 4 weeks	21021901LJ	3	1036
RVΔL-Cre: 4 weeks	21021901LJ	4	1195
RVΔL-Cre: 4 weeks	21021901LJ	5	1402
RVΔL-Cre: 4 weeks	21021901LJ	6	1739

RVΔL-Cre: 4 weeks	21021901LJ	7	1793
RVΔL-Cre: 4 weeks	21021901LJ	8	1913
RVΔL-Cre: 4 weeks	21021901LJ	9	2026
RVΔL-Cre: 4 weeks	21021901LJ	10	1913
RVΔL-Cre: 4 weeks	21021901LJ	11	1929
RVΔL-Cre: 4 weeks	21021901LJ	12	1668
RVΔL-Cre: 4 weeks	21021901LJ	13	1247
RVΔL-Cre: 4 weeks	21021901LJ	14	1062
RVΔL-Cre: 4 weeks	21021901LJ	15	874
RVΔL-Cre: 4 weeks	21021901LJ	total:	21743
RVΔL-Cre: 4 weeks	21021902LJ	1	1357
RVΔL-Cre: 4 weeks	21021902LJ	2	1416
RVΔL-Cre: 4 weeks	21021902LJ	3	1287
RVΔL-Cre: 4 weeks	21021902LJ	4	1308
RVΔL-Cre: 4 weeks	21021902LJ	5	1583
RVΔL-Cre: 4 weeks	21021902LJ	6	1850
RVΔL-Cre: 4 weeks	21021902LJ	7	2020
RVΔL-Cre: 4 weeks	21021902LJ	8	2238
RVΔL-Cre: 4 weeks	21021902LJ	9	2092
RVΔL-Cre: 4 weeks	21021902LJ	10	2321
RVΔL-Cre: 4 weeks	21021902LJ	11	2241
RVΔL-Cre: 4 weeks	21021902LJ	12	1858
RVΔL-Cre: 4 weeks	21021902LJ	13	1326
RVΔL-Cre: 4 weeks	21021902LJ	14	1083
RVΔL-Cre: 4 weeks	21021902LJ	15	793
RVΔL-Cre: 4 weeks	21021902LJ	total:	24773
RVΔL-Cre: 4 weeks	21021903LJ	1	1543
RVΔL-Cre: 4 weeks	21021903LJ	2	1406
RVΔL-Cre: 4 weeks	21021903LJ	3	1303
RVΔL-Cre: 4 weeks	21021903LJ	4	1489
RVΔL-Cre: 4 weeks	21021903LJ	5	1825
RVΔL-Cre: 4 weeks	21021903LJ	6	1946
RVΔL-Cre: 4 weeks	21021903LJ	7	1924
RVΔL-Cre: 4 weeks	21021903LJ	8	2142
RVΔL-Cre: 4 weeks	21021903LJ	9	2077
RVΔL-Cre: 4 weeks	21021903LJ	10	1954
RVΔL-Cre: 4 weeks	21021903LJ	11	1672
RVΔL-Cre: 4 weeks	21021903LJ	12	1411
RVΔL-Cre: 4 weeks	21021903LJ	13	1020
RVΔL-Cre: 4 weeks	21021903LJ	14	687
RVΔL-Cre: 4 weeks	21021903LJ	15	627
RVΔL-Cre: 4 weeks	21021903LJ	total:	23026
RVΔL-Cre: 4 weeks	21021904LJ	1	1592
RVΔL-Cre: 4 weeks	21021904LJ	2	1466
RVΔL-Cre: 4 weeks	21021904LJ	3	1355
RVΔL-Cre: 4 weeks	21021904LJ	4	1599
RVΔL-Cre: 4 weeks	21021904LJ	5	1736
RVΔL-Cre: 4 weeks	21021904LJ	6	1862
RVΔL-Cre: 4 weeks	21021904LJ	7	1794
RVΔL-Cre: 4 weeks	21021904LJ	8	1930
RVΔL-Cre: 4 weeks	21021904LJ	9	2047
RVΔL-Cre: 4 weeks	21021904LJ	10	1584
RVΔL-Cre: 4 weeks	21021904LJ	11	1755
RVΔL-Cre: 4 weeks	21021904LJ	12	1431
RVΔL-Cre: 4 weeks	21021904LJ	13	741

RVΔL-Cre: 4 weeks	21021904LJ	14	755
RVΔL-Cre: 4 weeks	21021904LJ	15	625
RVΔL-Cre: 4 weeks	21021904LJ	total:	22272
RVΔL-5tTA: 1 week	21042901LJ	3	2
RVΔL-5tTA: 1 week	21042901LJ	6	9
RVΔL-5tTA: 1 week	21042901LJ	7	4
RVΔL-5tTA: 1 week	21042901LJ	8	26
RVΔL-5tTA: 1 week	21042901LJ	9	32
RVΔL-5tTA: 1 week	21042901LJ	10	54
RVΔL-5tTA: 1 week	21042901LJ	11	69
RVΔL-5tTA: 1 week	21042901LJ	12	56
RVΔL-5tTA: 1 week	21042901LJ	13	51
RVΔL-5tTA: 1 week	21042901LJ	14	14
RVΔL-5tTA: 1 week	21042901LJ	15	22
RVΔL-5tTA: 1 week	21042901LJ	total:	339
RVΔL-5tTA: 1 week	21042902LJ	1	4
RVΔL-5tTA: 1 week	21042902LJ	2	11
RVΔL-5tTA: 1 week	21042902LJ	3	14
RVΔL-5tTA: 1 week	21042902LJ	4	4
RVΔL-5tTA: 1 week	21042902LJ	5	39
RVΔL-5tTA: 1 week	21042902LJ	6	108
RVΔL-5tTA: 1 week	21042902LJ	7	213
RVΔL-5tTA: 1 week	21042902LJ	8	255
RVΔL-5tTA: 1 week	21042902LJ	9	296
RVΔL-5tTA: 1 week	21042902LJ	10	219
RVΔL-5tTA: 1 week	21042902LJ	11	134
RVΔL-5tTA: 1 week	21042902LJ	12	64
RVΔL-5tTA: 1 week	21042902LJ	13	29
RVΔL-5tTA: 1 week	21042902LJ	14	14
RVΔL-5tTA: 1 week	21042902LJ	15	7
RVΔL-5tTA: 1 week	21042902LJ	total:	1411
RVΔL-5tTA: 1 week	21042903LJ	2	3
RVΔL-5tTA: 1 week	21042903LJ	3	7
RVΔL-5tTA: 1 week	21042903LJ	4	6
RVΔL-5tTA: 1 week	21042903LJ	5	4
RVΔL-5tTA: 1 week	21042903LJ	6	27
RVΔL-5tTA: 1 week	21042903LJ	7	40
RVΔL-5tTA: 1 week	21042903LJ	8	81
RVΔL-5tTA: 1 week	21042903LJ	9	115
RVΔL-5tTA: 1 week	21042903LJ	10	165
RVΔL-5tTA: 1 week	21042903LJ	11	120
RVΔL-5tTA: 1 week	21042903LJ	12	84
RVΔL-5tTA: 1 week	21042903LJ	13	67
RVΔL-5tTA: 1 week	21042903LJ	14	44
RVΔL-5tTA: 1 week	21042903LJ	15	33
RVΔL-5tTA: 1 week	21042903LJ	total:	796
RVΔL-5tTA: 1 week	21060301LJ	1	85
RVΔL-5tTA: 1 week	21060301LJ	2	117
RVΔL-5tTA: 1 week	21060301LJ	3	154
RVΔL-5tTA: 1 week	21060301LJ	4	59
RVΔL-5tTA: 1 week	21060301LJ	5	207
RVΔL-5tTA: 1 week	21060301LJ	6	325
RVΔL-5tTA: 1 week	21060301LJ	7	314
RVΔL-5tTA: 1 week	21060301LJ	8	303
RVΔL-5tTA: 1 week	21060301LJ	9	288

RVΔL-5tTA: 1 week	21060301LJ	10	185
RVΔL-5tTA: 1 week	21060301LJ	11	141
RVΔL-5tTA: 1 week	21060301LJ	12	47
RVΔL-5tTA: 1 week	21060301LJ	13	19
RVΔL-5tTA: 1 week	21060301LJ	14	14
RVΔL-5tTA: 1 week	21060301LJ	15	13
RVΔL-5tTA: 1 week	21060301LJ	total:	2271
RVΔL-5tTA: 4 weeks	21042905LJ	1	4
RVΔL-5tTA: 4 weeks	21042905LJ	2	14
RVΔL-5tTA: 4 weeks	21042905LJ	3	6
RVΔL-5tTA: 4 weeks	21042905LJ	4	21
RVΔL-5tTA: 4 weeks	21042905LJ	5	15
RVΔL-5tTA: 4 weeks	21042905LJ	6	41
RVΔL-5tTA: 4 weeks	21042905LJ	7	42
RVΔL-5tTA: 4 weeks	21042905LJ	8	101
RVΔL-5tTA: 4 weeks	21042905LJ	9	156
RVΔL-5tTA: 4 weeks	21042905LJ	10	109
RVΔL-5tTA: 4 weeks	21042905LJ	11	94
RVΔL-5tTA: 4 weeks	21042905LJ	12	24
RVΔL-5tTA: 4 weeks	21042905LJ	13	87
RVΔL-5tTA: 4 weeks	21042905LJ	14	44
RVΔL-5tTA: 4 weeks	21042905LJ	15	71
RVΔL-5tTA: 4 weeks	21042905LJ	total:	829
RVΔL-5tTA: 4 weeks	21042906LJ	1	9
RVΔL-5tTA: 4 weeks	21042906LJ	2	17
RVΔL-5tTA: 4 weeks	21042906LJ	3	28
RVΔL-5tTA: 4 weeks	21042906LJ	4	23
RVΔL-5tTA: 4 weeks	21042906LJ	5	24
RVΔL-5tTA: 4 weeks	21042906LJ	6	25
RVΔL-5tTA: 4 weeks	21042906LJ	7	93
RVΔL-5tTA: 4 weeks	21042906LJ	8	200
RVΔL-5tTA: 4 weeks	21042906LJ	9	305
RVΔL-5tTA: 4 weeks	21042906LJ	10	233
RVΔL-5tTA: 4 weeks	21042906LJ	11	200
RVΔL-5tTA: 4 weeks	21042906LJ	12	141
RVΔL-5tTA: 4 weeks	21042906LJ	13	74
RVΔL-5tTA: 4 weeks	21042906LJ	14	108
RVΔL-5tTA: 4 weeks	21042906LJ	15	94
RVΔL-5tTA: 4 weeks	21042906LJ	total:	1574
RVΔL-5tTA: 4 weeks	21042907LJ	2	2
RVΔL-5tTA: 4 weeks	21042907LJ	4	3
RVΔL-5tTA: 4 weeks	21042907LJ	5	5
RVΔL-5tTA: 4 weeks	21042907LJ	6	24
RVΔL-5tTA: 4 weeks	21042907LJ	7	32
RVΔL-5tTA: 4 weeks	21042907LJ	8	51
RVΔL-5tTA: 4 weeks	21042907LJ	9	100
RVΔL-5tTA: 4 weeks	21042907LJ	10	74
RVΔL-5tTA: 4 weeks	21042907LJ	11	69
RVΔL-5tTA: 4 weeks	21042907LJ	12	54
RVΔL-5tTA: 4 weeks	21042907LJ	13	26
RVΔL-5tTA: 4 weeks	21042907LJ	14	31
RVΔL-5tTA: 4 weeks	21042907LJ	15	28
RVΔL-5tTA: 4 weeks	21042907LJ	total:	499
RVΔL-5tTA: 4 weeks	21042908LJ	1	64
RVΔL-5tTA: 4 weeks	21042908LJ	2	67

RVΔL-5tTA: 4 weeks	21042908LJ	3	66
RVΔL-5tTA: 4 weeks	21042908LJ	4	79
RVΔL-5tTA: 4 weeks	21042908LJ	5	151
RVΔL-5tTA: 4 weeks	21042908LJ	6	149
RVΔL-5tTA: 4 weeks	21042908LJ	7	166
RVΔL-5tTA: 4 weeks	21042908LJ	8	171
RVΔL-5tTA: 4 weeks	21042908LJ	9	184
RVΔL-5tTA: 4 weeks	21042908LJ	10	57
RVΔL-5tTA: 4 weeks	21042908LJ	11	48
RVΔL-5tTA: 4 weeks	21042908LJ	12	29
RVΔL-5tTA: 4 weeks	21042908LJ	13	14
RVΔL-5tTA: 4 weeks	21042908LJ	14	27
RVΔL-5tTA: 4 weeks	21042908LJ	15	57
RVΔL-5tTA: 4 weeks	21042908LJ	total:	1329

Condition	Mouse number	Cell counts
RVΔGL-Flpo: 1 week	21021505LJ	22
RVΔGL-Flpo: 1 week	21021506LJ	18
RVΔGL-Flpo: 1 week	21021507LJ	121
RVΔGL-Flpo: 1 week	21021508LJ	2
RVΔGL-Flpo: 1 week	21052505LJ	7
RVΔGL-Flpo: 1 week	21052506LJ	8
RVΔGL-Flpo: 1 week	21052507LJ	98
RVΔGL-Flpo: 1 week	21052508LJ	6
RVΔGL-Flpo: 1 week	Mean:	35.25
RVΔL-Flpo: 1 week	21021805LJ	3093
RVΔL-Flpo: 1 week	21021806LJ	320
RVΔL-Flpo: 1 week	21021807LJ	311
RVΔL-Flpo: 1 week	21021808LJ	263
RVΔL-Flpo: 1 week	21052607LJ	47
RVΔL-Flpo: 1 week	21052608LJ	2161
RVΔL-Flpo: 1 week	21060302LJ	365
RVΔL-Flpo: 1 week	21060303LJ	238
RVΔL-Flpo: 1 week	Mean:	849.75
RVΔGL-Flpo: 4 weeks	21021501LJ	80
RVΔGL-Flpo: 4 weeks	21021502LJ	62
RVΔGL-Flpo: 4 weeks	21021503LJ	3254
RVΔGL-Flpo: 4 weeks	21021504LJ	237
RVΔGL-Flpo: 4 weeks	21052501LJ	43
RVΔGL-Flpo: 4 weeks	21052502LJ	14
RVΔGL-Flpo: 4 weeks	21052503LJ	130
RVΔGL-Flpo: 4 weeks	21052504LJ	65
RVΔGL-Flpo: 4 weeks	Mean:	485.625
RVΔL-Flpo: 4 weeks	21021801LJ	4614
RVΔL-Flpo: 4 weeks	21021802LJ	3006
RVΔL-Flpo: 4 weeks	21021803LJ	1847
RVΔL-Flpo: 4 weeks	21021804LJ	3331
RVΔL-Flpo: 4 weeks	21052601LJ	1369
RVΔL-Flpo: 4 weeks	21052602LJ	2919
RVΔL-Flpo: 4 weeks	21052603LJ	3730
RVΔL-Flpo: 4 weeks	21052606LJ	3454
RVΔL-Flpo: 4 weeks	Mean:	3033.75
RVΔGL-Cre: 1 week	21021703LJ	13484
RVΔGL-Cre: 1 week	21021704LJ	14635
RVΔGL-Cre: 1 week	21021707LJ	10647
RVΔGL-Cre: 1 week	21021708LJ	10845
RVΔGL-Cre: 1 week	Mean:	12402.75
RVΔL-Cre: 1 week	21021905LJ	16907
RVΔL-Cre: 1 week	21021906LJ	17923
RVΔL-Cre: 1 week	21021907LJ	18751
RVΔL-Cre: 1 week	21021908LJ	16257
RVΔL-Cre: 1 week	Mean:	17459.5
RVΔGL-Cre: 4 weeks	21021701LJ	19156
RVΔGL-Cre: 4 weeks	21021702LJ	17935
RVΔGL-Cre: 4 weeks	21021705LJ	18539
RVΔGL-Cre: 4 weeks	21021706LJ	17938
RVΔGL-Cre: 4 weeks	Mean:	18392
RVΔL-Cre: 4 weeks	21021901LJ	21743
RVΔL-Cre: 4 weeks	21021902LJ	24773
RVΔL-Cre: 4 weeks	21021903LJ	23026
RVΔL-Cre: 4 weeks	21021904LJ	22272
RVΔL-Cre: 4 weeks	Mean:	22953.5
RVΔL-5tTA: 1 week	21042901LJ	339
RVΔL-5tTA: 1 week	21042902LJ	1411
RVΔL-5tTA: 1 week	21042903LJ	796
RVΔL-5tTA: 1 week	21060301LJ	2271
RVΔL-5tTA: 1 week	Mean:	1204.25
RVΔL-5tTA: 4 weeks	21042905LJ	829
RVΔL-5tTA: 4 weeks	21042906LJ	1574
RVΔL-5tTA: 4 weeks	21042907LJ	499
RVΔL-5tTA: 4 weeks	21042908LJ	1329
RVΔL-5tTA: 4 weeks	Mean:	1057.75

RVΔGL-Flpo 4 weeks	RVΔL-Flpo 4 weeks
80	4614
62	3006
3254	1847
237	3331
43	1369
14	2919
130	3730
65	3454

Anova: Single Factor

SUMMARY

Groups	*Count*	*Sum*	*Average*	*Variance*
RVΔGL-Flpo 4 weeks	8	3885	485.625	1255920.84
RVΔL-Flpo 4 weeks	8	24270	3033.75	1062946.79

ANOVA

Source of Variation	*SS*	*df*	*MS*	*F*	*P-value*	*F crit*
Between Groups	25971764.06	1	25971764.1	22.4003852	0.00032063	4.60010994
Within Groups	16232073.38	14	1159433.81			
Total	42203837.44	15				

RVΔGL-Flpo 1 week	RVΔGL-Flpo 4 weeks
22	80
18	62
121	3254
2	237
7	43
8	14
98	130
6	65

Anova: Single Factor

SUMMARY

Groups	*Count*	*Sum*	*Average*	*Variance*
RVΔGL-Flpo 1 week	8	282	35.25	2180.78571
RVΔGL-Flpo 4 weeks	8	3885	485.625	1255920.84

ANOVA

Source of Variation	*SS*	*df*	*MS*	*F*	*P-value*	*F crit*
Between Groups	811350.5625	1	811350.563	1.28980131	0.27515341	4.60010994
Within Groups	8806711.375	14	629050.813			
Total	9618061.938	15				

RVΔGL-Flpo 4 weeks	RVΔL-Flpo 1 week
80	3093
62	320
3254	311
237	263

Anova: Single Factor

SUMMARY

Groups	*Count*	*Sum*	*Average*	*Variance*
RVΔGL-Flpo 4 weeks	4	3633	908.25	2451752.25
RVΔL-Flpo 1 week	4	3987	996.75	1953632.25

ANOVA

Source of Variation	*SS*	*df*	*MS*	*F*	*P-value*	*F crit*
Between Groups	15664.5	1	15664.5	0.00711152	0.93553752	5.98737761
Within Groups	13216153.5	6	2202692.25			
Total	13231818	7				

RVΔL-Flpo 4 weeks	RVΔGL-Flpo 1 week
4614	22
3006	18
1847	121
3331	2

Anova: Single Factor

SUMMARY

Groups	*Count*	*Sum*	*Average*	*Variance*
RVΔL-Flpo 4 weeks	4	12798	3199.5	1294933.67
RVΔGL-Flpo 1 week	4	163	40.75	2936.91667

ANOVA

Source of Variation	*SS*	*df*	*MS*	*F*	*P-value*	*F crit*
Between Groups	19955403.13	1	19955403.1	30.7509907	0.00145233	5.98737761
Within Groups	3893611.75	6	648935.292			
Total	23849014.88	7				

RVΔL-Flpo 1 week	RVΔL-Flpo 4 weeks
3093	4614
320	3006
311	1847
263	3331
47	1369
2161	2919
365	3730
238	3454

Anova: Single Factor

SUMMARY

Groups	*Count*	*Sum*	*Average*	*Variance*
RVΔL-Flpo 1 week	8	6798	849.75	1274333.93
RVΔL-Flpo 4 weeks	8	24270	3033.75	1062946.79

ANOVA

Source of Variation	*SS*	*df*	*MS*	*F*	*P-value*	*F crit*
Between Groups	19079424	1	19079424	16.3261724	0.00121549	4.60010994
Within Groups	16360965	14	1168640.36			
Total	35440389	15				

RVΔGL-Flpo 1 week	RVΔL-Flpo 1 week
22	3093
18	320
121	311
2	263
7	47
8	2161
98	365
6	238

Anova: Single Factor

SUMMARY

Groups	*Count*	*Sum*	*Average*	*Variance*
RVΔGL-Flpo 1 week	8	282	35.25	2180.78571
RVΔL-Flpo 1 week	8	6798	849.75	1274333.93

ANOVA

Source of Variation	*SS*	*df*	*MS*	*F*	*P-value*	*F crit*
Between Groups	2653641	1	2653641	4.1576348	0.06079134	4.60010994
Within Groups	8935603	14	638257.357			
Total	11589244	15				

RVΔGL-Cre 4 weeks	RVΔL-Cre 4 weeks
19156	21743
17935	24773
18539	23026
17938	22272

Anova: Single Factor

SUMMARY

Groups	*Count*	*Sum*	*Average*	*Variance*
RVΔGL-Cre 4 weeks	4	73568	18392	340090
RVΔL-Cre 4 weeks	4	91814	22953.5	1748529.67

ANOVA

Source of Variation	SS	df	MS	F	P-value	F crit
Between Groups	41614564.5	1	41614564.5	39.8488678	0.00073769	5.98737761
Within Groups	6265859	6	1044309.83			
Total	47880423.5	7				

RVΔGL-Cre 4 weeks	RVΔGL-Cre 1 week
19156	13484
17935	14635
18539	10647
17938	10845

Anova: Single Factor

SUMMARY

Groups	*Count*	*Sum*	*Average*	*Variance*
RVΔGL-Cre 4 weeks	4	73568	18392	340090
RVΔGL-Cre 1 week	4	49611	12402.75	3887094.92

ANOVA

Source of Variation	*SS*	*df*	*MS*	*F*	*P-value*	*F crit*
Between Groups	71742231.13	1	71742231.1	33.943266	0.00112486	5.98737761
Within Groups	12681554.75	6	2113592.46			
Total	84423785.88	7				

RVΔGL-Cre 4 weeks	RVΔL-Cre 1 week
19156	16907
17935	17923
18539	18751
17938	16257

Anova: Single Factor

SUMMARY

Groups	*Count*	*Sum*	*Average*	*Variance*
RVΔGL-Cre 4 weeks	4	73568	18392	340090
RVΔL-Cre 1 week	4	69838	17459.5	1211355.67

ANOVA

Source of Variation	*SS*	*df*	*MS*	*F*	*P-value*	*F crit*
Between Groups	1739112.5	1	1739112.5	2.24192511	0.1849584	5.98737761
Within Groups	4654337	6	775722.833			
Total	6393449.5	7				

RVΔL-Cre 4 weeks	RVΔGL-Cre 1 week
21743	13484
24773	14635
23026	10647
22272	10845

Anova: Single Factor

SUMMARY

Groups	*Count*	*Sum*	*Average*	*Variance*
RVΔL-Cre 4 weeks	4	91814	22953.5	1748529.67
RVΔGL-Cre 1 week	4	49611	12402.75	3887094.92

ANOVA

Source of Variation	*SS*	*df*	*MS*	*F*	*P-value*	*F crit*
Between Groups	222636651.1	1	222636651	79.010462	0.00011291	5.98737761
Within Groups	16906873.75	6	2817812.29			
Total	239543524.9	7				

RVΔL-Cre 4 weeks	RVΔL-Cre 1 week
21743	16907
24773	17923
23026	18751
22272	16257

Anova: Single Factor

SUMMARY

Groups	*Count*	*Sum*	*Average*	*Variance*
RVΔL-Cre 4 weeks	4	91814	22953.5	1748529.67
RVΔL-Cre 1 week	4	69838	17459.5	1211355.67

ANOVA

Source of Variation	*SS*	*df*	*MS*	*F*	*P-value*	*F crit*
Between Groups	60368072	1	60368072	40.790818	0.00069327	5.98737761
Within Groups	8879656	6	1479942.67			
Total	69247728	7				

RVΔGL-Cre 1 week	RVΔL-Cre 1 week
13484	16907
14635	17923
10647	18751
10845	16257

Anova: Single Factor

SUMMARY

Groups	*Count*	*Sum*	*Average*	*Variance*
RVΔGL-Cre 1 week	4	49611	12402.75	3887094.92
RVΔL-Cre 1 week	4	69838	17459.5	1211355.67

ANOVA

Source of Variation	*SS*	*df*	*MS*	*F*	*P-value*	*F crit*
Between Groups	51141441.13	1	51141441.1	20.061562	0.00419681	5.98737761
Within Groups	15295351.75	6	2549225.29			
Total	66436792.88	7				

RVΔL-5tTA 1 week	RVΔL-5tTA 4 weeks
339	829
1411	1574
796	499
2271	1329

Anova: Single Factor

SUMMARY

Groups	*Count*	*Sum*	*Average*	*Variance*
RVΔL-5tTA 1 week	4	4817	1204.25	698675.583
RVΔL-5tTA 4 weeks	4	4231	1057.75	234872.917

ANOVA

Source of Variation	*SS*	*df*	*MS*	*F*	*P-value*	*F crit*
Between Groups	42924.5	1	42924.5	0.09195987	0.77193993	5.98737761
Within Groups	2800645.5	6	466774.25			
Total	2843570	7				

Comparison	p-value
RVΔGL-Flpo 4 weeks vs RVΔL-Flpo 4 weeks	**0.000320625**
RVΔGL-Flpo 4 weeks vs RVΔGL-Flpo 1 week	0.27515341
RVΔGL-Flpo 4 weeks vs RVΔL-Flpo 1 week	0.93553752
RVΔL-Flpo 4 weeks vs RVΔGL-Flpo 1 week	**0.001452333**
RVΔL-Flpo 4 weeks vs RVΔL-Flpo 1 week	**0.001215493**
RVΔGL-Flpo 1 week vs RVΔL-Flpo 1 week	0.060791343
RVΔGL-Cre 4 weeks vs RVΔL-Cre 4 weeks	**0.000737695**
RVΔGL-Cre 4 weeks vs RVΔGL-Cre 1 week	**0.001124862**
RVΔGL-Cre 4 weeks vs RVΔL-Cre 1 weeks	0.184958403
RVΔL-Cre 4 weeks vs RVΔGL-Cre 1 week	**0.000112909**
RVΔL-Cre 4 weeks vs RVΔL-Cre 1 week	**0.000693266**
RVΔGL-Cre 1 week vs RVΔL-Cre 1 week	**0.004196815**
RVΔL-5tTA 1 week vs RVΔL-5tTA 4 weeks	0.77193993

Video S1. RV∆L-Cre-labeled cortical neurons at 2 weeks vs 10 weeks postinjection, Related to Figure 3

3-dimensional rendering of the same cortical volume shown in Figure 3, panel B.

See external file.

File S3. Cell counts and statistics for structural two-photon imaging experiments, Related to Figure 3

See following pages.

RVΔGL-Cre: cell counts	Animal-1 FOV-1	Animal-1 FOV-2	Animal-2 FOV-1	Animal-2 FOV-2	Animal-3 FOV-1	Animal-3 FOV-2	Animal-4 FOV-1	Animal-4 FOV-2
Week-1	300	315	219	318	435	288	203	220
Week-2	519	359	269	546	488	364	321	354
Week-3	537	390	305	569	505	443	369	427
Week-4	538	403	317	572	518	445	372	426
Week-6	537	403	319	571	515	451	370	424
Week-12	535	400	319	567	514	443	369	424
Week-14			319	567	513	442	368	421
Week-16			319					

RVΔGL-Cre: percentage to week-1	Animal-1 FOV-1	Animal-1 FOV-2	Animal-2 FOV-1	Animal-2 FOV-2	Animal-3 FOV-1	Animal-3 FOV-2	Animal-4 FOV-1	Animal-4 FOV-2
Week-1	1.00	1.00	1.00	1.00	1.00	1.00	1.00	1.00
Week-2	1.73	1.14	1.23	1.72	1.12	1.26	1.58	1.61
Week-3	1.79	1.24	1.39	1.79	1.16	1.54	1.82	1.94
Week-4	1.79	1.28	1.45	1.80	1.19	1.55	1.83	1.94
Week-6	1.79	1.28	1.46	1.80	1.18	1.57	1.82	1.93
Week-12	1.78	1.27	1.46	1.78	1.18	1.54	1.82	1.93
Week-14			1.46	1.78	1.18	1.53	1.81	1.91
Week-16			1.46					

RVΔGL-Cre: comparison between week-1 and week-4	Animal-1 FOV-1	Animal-1 FOV-2	Animal-2 FOV-1	Animal-2 FOV-2	Animal-3 FOV-1	Animal-3 FOV-2	Animal-4 FOV-1	Animal-4 FOV-2
Week-1	300	315	219	318	435	288	203	220
Week-4	538	403	317	572	518	445	372	426
Increase (Week-4 - Week-1)	238	88	98	254	83	157	169	206
% increase (Week-4 - Week-1)	79.33%	27.94%	44.75%	79.87%	19.08%	54.51%	83.25%	93.64%
Increase (Week-12 - Week-4)	-3	-3	2	-5	-4	-2	-3	-2
% increase (Week-12 - Week-4)	-0.56%	-0.74%	0.63%	-0.87%	-0.77%	-0.45%	-0.81%	-0.47%

t-Test: Paired Two Sample for Means		
	Week-1	Week-4
Mean	287.25	448.875
Variance	5712.5	7689.267857
Observations	8	8
Pearson Correlation	0.665513457	
Hypothesized Mean Difference	0	
df	7	
t Stat	-6.75473154	
P(T<=t) one-tail	**0.000131934**	
t Critical one-tail	1.894578605	
P(T<=t) two-tail	0.000263868	
t Critical two-tail	2.364624252	

t-Test: Paired Two Sample for Means		
	Week-4	Week-12
Mean	448.875	446.375
Variance	7689.267857	7407.410714
Observations	8	8
Pearson Correlation	0.999890399	
Hypothesized Mean Difference	0	
df	7	
t Stat	3.415650255	
P(T<=t) one-tail	**0.005600716**	
t Critical one-tail	1.894578605	
P(T<=t) two-tail	0.011201433	
t Critical two-tail	2.364624252	

% increase from 1 week to 4 weeks:								
RVΔGL-Cre	79.33%	27.94%	44.75%	79.87%	19.08%	54.51%	83.25%	93.64%
RVΔL-Cre	84.38%	84.41%	49.57%	70.25%	54.88%	67.66%	40.66%	93.26%

Unpaired t test	
Table Analyzed	% increase
P value	**0.5187**
P value summary	ns
Significantly different (P < 0.05)?	No
One- or two-tailed P value?	Two-tailed
t, df	t=0.6621, df=14
How big is the difference?	
Mean of RVΔGL-Cre	0.603
Mean of RVΔL-Cre	0.6813
Difference between means (B - A) ± SEM	0.07836 ± 0.1184
95% confidence interval	-0.1755 to 0.3322
R squared (eta squared)	0.03036
F test to compare variances	
F, DFn, Dfd	2.216, 7, 7
P value	0.3158
P value summary	ns
Significantly different (P < 0.05)?	No
Data analyzed	
Sample size, RVΔGL-Cre	8
Sample size, RVΔL-Cre	8

% increase from 4 weeks to 12 weeks:								
RVΔGL-Cre	-0.56%	-0.74%	0.63%	-0.87%	-0.77%	-0.45%	-0.81%	-0.47%
RVΔL-Cre	0.48%	-0.29%	2.31%	-1.46%	3.30%	0.00%	0.78%	0.58%

Unpaired t test	
P value	**0.0451**
P value summary	*
Significantly different (P < 0.05)?	Yes
One- or two-tailed P value?	Two-tailed
t, df	t=2.199, df=14
How big is the difference?	
Mean of RVΔGL-Cre	-0.005054
Mean of RVΔL-Cre	0.007135
Difference between means (B - A) ± SEM	.01219 ± 0.005542
95% confidence interval	0003030 to 0.02407
R squared (eta squared)	0.2568
F test to compare variances	
F, DFn, Dfd	9.402, 7, 7
P value	0.0085
P value summary	**
Significantly different (P < 0.05)?	Yes
Data analyzed	
Sample size, RVΔGL-Cre	8
Sample size, RVΔL-Cre	8

RVΔL-Cre: cell counts	Animal-1 FOV-1	Animal-1 FOV-2	Animal-2 FOV-1	Animal-2 FOV-2	Animal-3 FOV-1	Animal-3 FOV-2	Animal-4 FOV-1	Animal-4 FOV-2
Week-1	224	186	232	242	215	167	182	178
Week-2	331	307	300	298	270	237	200	228
Week-3	396	340	341	378	289	279	253	304
Week-4	413	343	347	412	333	280	256	344
Week-6	409	342	347	413	342	283	255	345
Week-12	415	342	355	406	344	280	258	346
Week 14	415	342	354	406	344	280		
Week-16				406	344	280		

RVΔL-Cre: percentage to week-1	Animal-1 FOV-1	Animal-1 FOV-2	Animal-2 FOV-1	Animal-2 FOV-2	Animal-3 FOV-1	Animal-3 FOV-2	Animal-4 FOV-1	Animal-4 FOV-2
Week-1	1.00	1.00	1.00	1.00	1.00	1.00	1.00	1.00
Week-2	1.48	1.65	1.29	1.23	1.26	1.42	1.10	1.28
Week-3	1.77	1.83	1.47	1.56	1.34	1.67	1.39	1.71
Week-4	1.84	1.84	1.50	1.70	1.55	1.68	1.41	1.93
Week-6	1.83	1.84	1.50	1.71	1.59	1.69	1.40	1.94
Week-12	1.85	1.84	1.53	1.68	1.60	1.68	1.42	1.94
Week 14	1.85	1.84	1.53	1.68	1.60	1.68		
Week-16				1.68	1.60	1.68		

RVΔL-Cre: comparison between week-1 and week-4	Animal-1 FOV-1	Animal-1 FOV-2	Animal-2 FOV-1	Animal-2 FOV-2	Animal-3 FOV-1	Animal-3 FOV-2	Animal-4 FOV-1	Animal-4 FOV-2
Week-1	224	186	232	242	215	167	182	178
Week-4	413	343	347	412	333	280	256	344
Increase (Week-4 - Week-1)	189	157	115	170	118	113	74	166
% increase (Week-4 - Week-1)	84.38%	84.41%	49.57%	70.25%	54.88%	67.66%	40.66%	93.26%
Increase (Week-12 - Week-4)	2	-1	8	-6	11	0	2	2
% increase (Week-12 - Week-4)	0.48%	-0.29%	2.31%	-1.46%	3.30%	0.00%	0.78%	0.58%

t-Test: Paired Two Sample for Means		
	Week-1	Week-4
Mean	203.25	341
Variance	799.6428571	3040.571429
Observations	8	8
Pearson Correlation	0.754099973	
Hypothesized Mean Difference	0	
df	7	
t Stat	-10.09862351	
P(T<=t) one-tail	**1.00266E-05**	
t Critical one-tail	1.894578605	
P(T<=t) two-tail	2.00531E-05	
t Critical two-tail	2.364624252	

t-Test: Paired Two Sample for Means		
	Week-4	Week-12
Mean	341	343.25
Variance	3040.571429	2928.785714
Observations	8	8
Pearson Correlation	0.995543784	
Hypothesized Mean Difference	0	
df	7	
t Stat	-1.210419877	
P(T<=t) one-tail	**0.13269902**	
t Critical one-tail	1.894578605	
P(T<=t) two-tail	0.265398039	
t Critical two-tail	2.364624252	

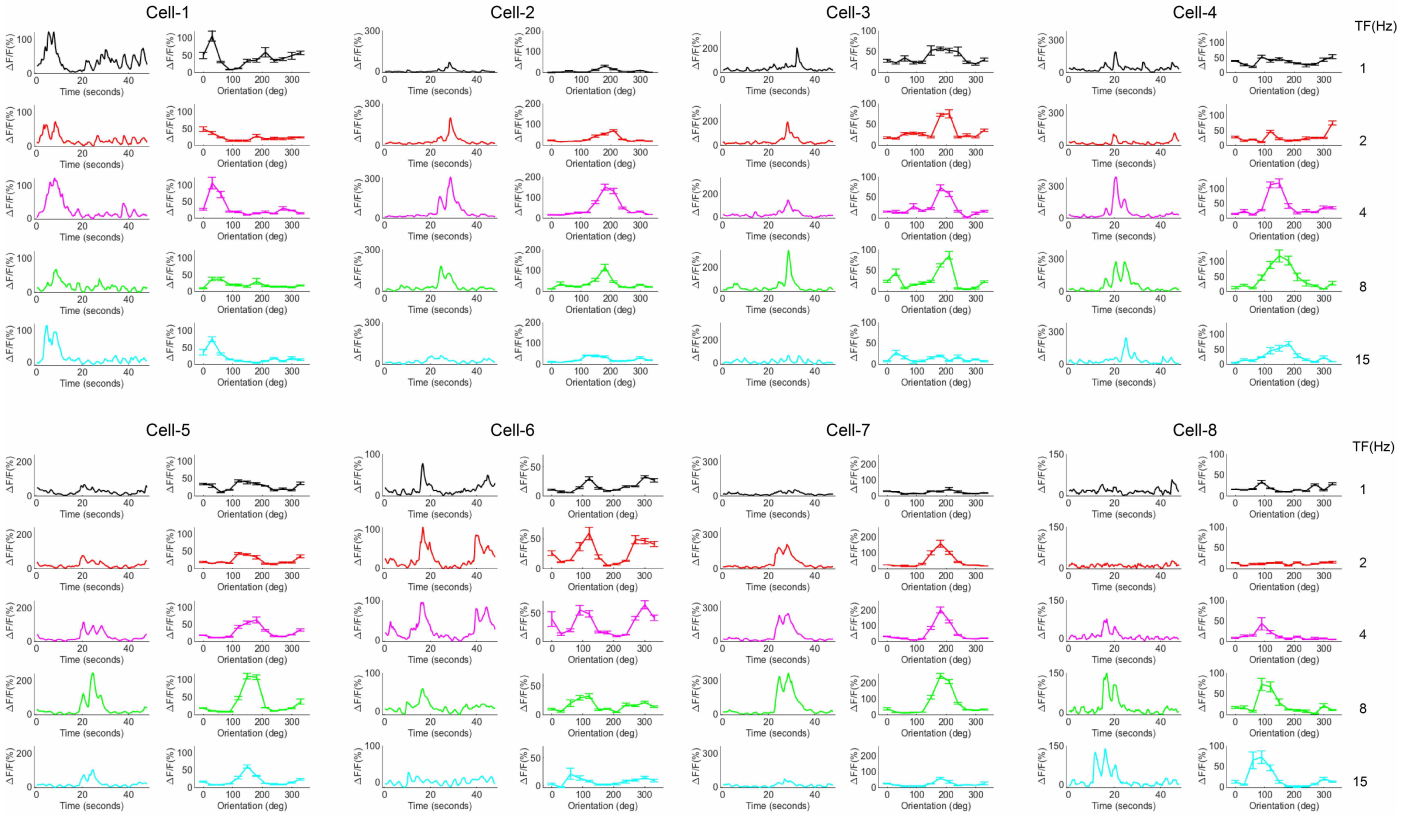

Figure S4. GCaMP6s signals and tuning curves of 8 example V1 neurons at 16 weeks postinjection, Related to Figure 4

These data were obtained with drifting gratings presented at 12 directions of motion and 5 temporal frequencies, repeated 10 times (tuning curve: mean ΔF/F ± s.e.m; GCaMP6s signals: mean ΔF/F) at two different FOVs at the 16-week timepoint.

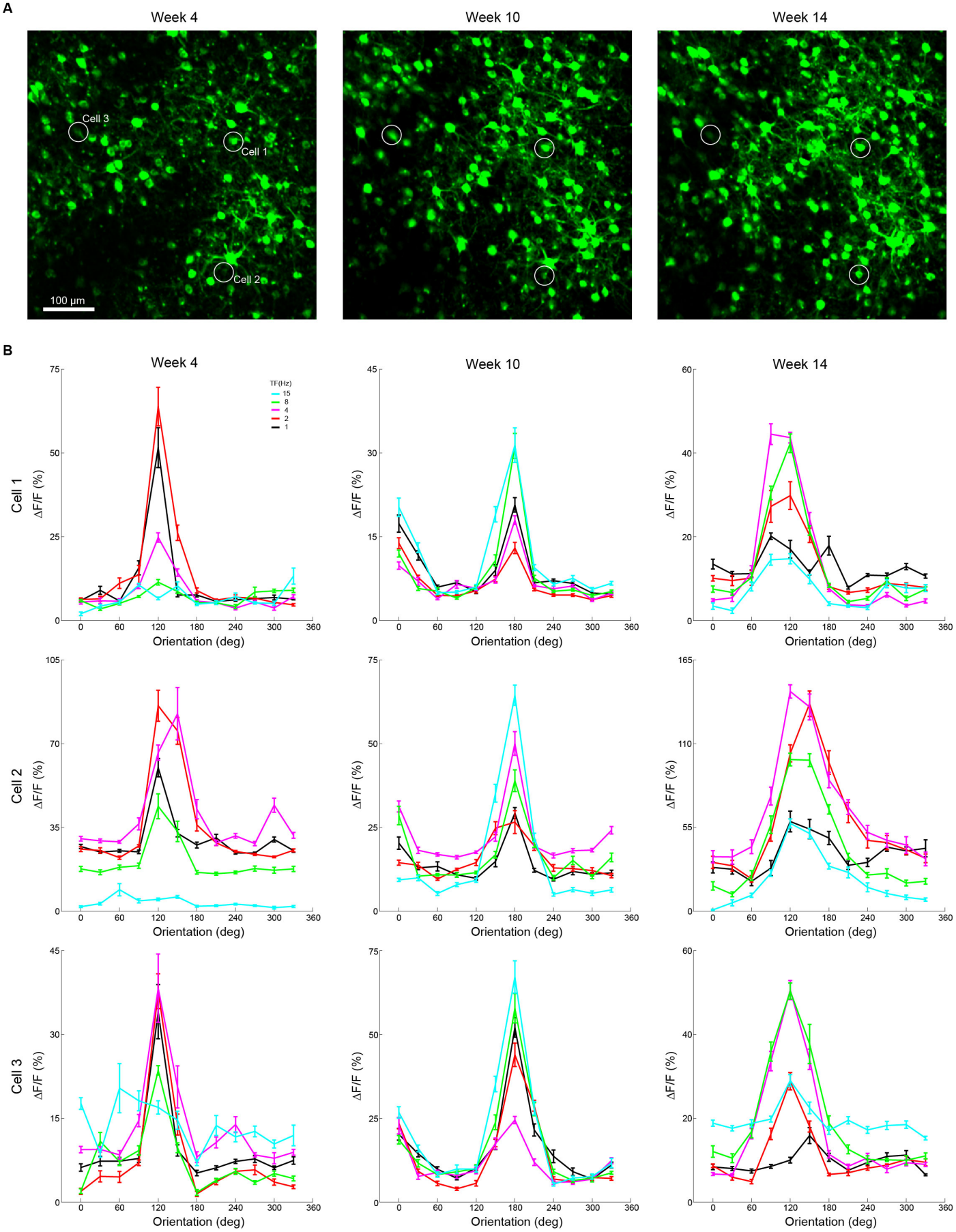

Figure S5. More examples showing long-term stability of orientation and temporal frequency tuning in RVΔL-Cre labeled neurons, Related to Figure 4

(A) Maximum intensity projections of the same FOV at 4 weeks, 10 weeks, and 14 weeks postinjection. Scale bar: 100 μm, applies to all images.
(B) Visual responses of the three circled cells in panel **a** measured at the three different timepoints. Data were obtained with drifting gratings presented at 12 directions of motion and 5 temporal frequencies (mean ΔF/F ± s.e.m., averaged over 10 repeats).

Video S2. GCaMP6s signals of visual cortical neurons 16 weeks after injection of RVΔL-Cre, Related to Figure 4

Video shows responses to 10 repeats of drifting gratings at 12 directions of motion at one temporal frequency (1 Hz) over a total of 480 seconds.

See external file.

File S4. Tuned cell counts and statistics for functional two-photon imaging experiments, Related to Figure 4

See following page.